International Journal of Earth Sciences (2023) 112:539–559
https://doi.org/10.1007/s00531-022-02270-6

ORIGINAL PAPER

Main drivers of drainage pattern development in onshore Makran Accretionary Wedge, SE Iran

Amaneh Kaveh-Firouz[1,2] · Ali Mohammadi[1,2] · Tolga Görüm[1] · Mehmet Akif Sarıkaya[1] · Hamid Alizadeh[2] · Abdullah Akbaş[3] · Ali Mirarabi[4]

Received: 6 July 2022 / Accepted: 7 November 2022 / Published online: 21 November 2022

Abstract
Over time, river networks achieve a specific pattern as determined by the function of several factors such as climate, tectonic, geological structures, topography, lithology, and base-level fluctuations. The relative importance of mentioned factors on drainage systems was studied to determine the controlling factors of their heterogeneity across the tectono-stratigraphic zones of onshore Iranian Makran. We applied structural, geomorphological, and climate analysis. Results indicate that the dendritic patterns of N-S flowing rivers in the western part of Iranian Makran are mostly controlled by the Minab-Zendan Fault activity and distribution of olistostrome cover, whereas the dominant trellis patterns in the eastern part are controlled by the well-developed thrust fault-related fold systems. The channel steepness pattern demonstrates that the high values are mostly localized in the hanging wall of thrust and normal faults. Accordingly, the topographic profiles of the steep rivers show the old stages of incision in the Inner and Outer Makran. However, some rivers of the Coastal Makran are in the young stage of incision, where the normal faults are located and active. The sediment connectivity index shows that the Inner Makran has a high potential of sediment supplies, while the Outer Makran intra-mountain basins and the Coastal-plain are more prone to sediments accumulation. Our findings reveal that the river patterns and landscape evolution in the Inner and Outer Makran are controlled by thrust faults, olistostrome and related mini-basins, while rivers in the Coastal Makran are governed by activity of Pliocene–Pleistocene normal faults.

Keywords Drainage pattern · Thrust-normal faults · Climatic-topographic analysis · Active accretionary wedge · Onshore Makran (Iran) · TanDEM-X 12.5 m

Introduction

The drainage networks are notable geomorphic features incised the Earth's surface, designed by uplift and erosion under the coupled impact of tectonics and climate (e.g. Howard 1967; Kirby and Whipple 2012; Willett et al. 2014; Seybold et al. 2021). The pattern of drainage networks and their evolution is useful in geological, structural, and geomorphological interpretations (e.g. Howard 1967; Twidale 2004). The presence of diverse drainage systems is important in terms of water-erosion hazards and environmental disasters such as flash-floods, mudflows, and debris flows especially in active continental margins (e.g. Montgomery and Dietrich 1989; Bull 2011). Drainage networks provide valuable information on fault system development and fold growth, and it may help to interpret the sedimentary basin geometry and sedimentation pattern based on the fault geometry (Jackson and Leeder 1994). The evolution of drainage patterns in active accretionary wedges largely depends on thrust faults (e.g. Viaplana-Muzas et al. 2015). In some cases, chaotic sedimentary cover (olistostrome) also influences drainage pattern by changing lithological strength (St-Onge 2012). Furthermore, extensional tectonic regime in mature active accretionary wedges generate normal faults (e.g. Ring et al. 2010), affecting drainage patterns. The Makran Accretionary

✉ Amaneh Kaveh-Firouz
amaneh.kaveh@gmail.com

1 Eurasia Institute of Earth Sciences, Istanbul Technical University, Maslak, Istanbul 34469, Turkey

2 Iranian National Institute for Oceanography and Atmospheric Sciences, Tehran, Iran

3 Geography Department, Physical Geography Division, Bursa Uludağ University, Bursa, Turkey

4 Water Resources Management Company, Tehran, Iran

Wedge is one of the largest active accretionary wedges in the world (Burg 2018) with arid/semi-arid climate settings (e.g. Kehl 2009) and almost 100% rock exposure with the presence of both thrust and normal faults, and olistostrome sedimentary cover (Dolati 2010).

The Makran Accretionary Wedge (Fig. 1a and inset) was formed during the Late Mesozoic by northward subduction of the Arabian Plate under the Central Iran and Afghan blocks (e.g. Ricou 1994; Alavi 2007). The Late Cretaceous-Oligocene deep marine sediment was supplied from the eroded Makran magmatic arc in the north, and Miocene deep to shallow marine-deltaic sediments was recycled from the exposed accretionary wedge (Mohammadi et al. 2016a, 2017). The accretionary wedge is divided into the onshore wedge to the north, and the active offshore (submarine) wedge to the south. These two parts are distincted by a narrow (a few kilometres wide) coastal belt where mud volcanoes and normal faults are noticeable in both onshore and offshore (e.g. Von Rad et al. 2000; Back and Morley 2016; Burg 2018). The onshore Makran Accretionary Wedge is partly exposed in SE Iran (e.g. McCall and Kidd 1982; McCall 2002) and in SW Pakistan (e.g. Farhoudi and Karig 1977; Leggett and Platt 1984), as well as offshore in the northern Arabian Sea (White and Louden 1982; White 1983).

Based on the seismic profiles across the eastern Makran, the offshore Makran consists of the outer deformation front and imbricate fan systems forming a series of thrust fault-related anticlinal ridges with interfering synclinal basins (thrust-top basins), along with an inner sector of the slope and upper slope where extensional normal faults and shale diapirs occur. In addition, four main depositional sequences

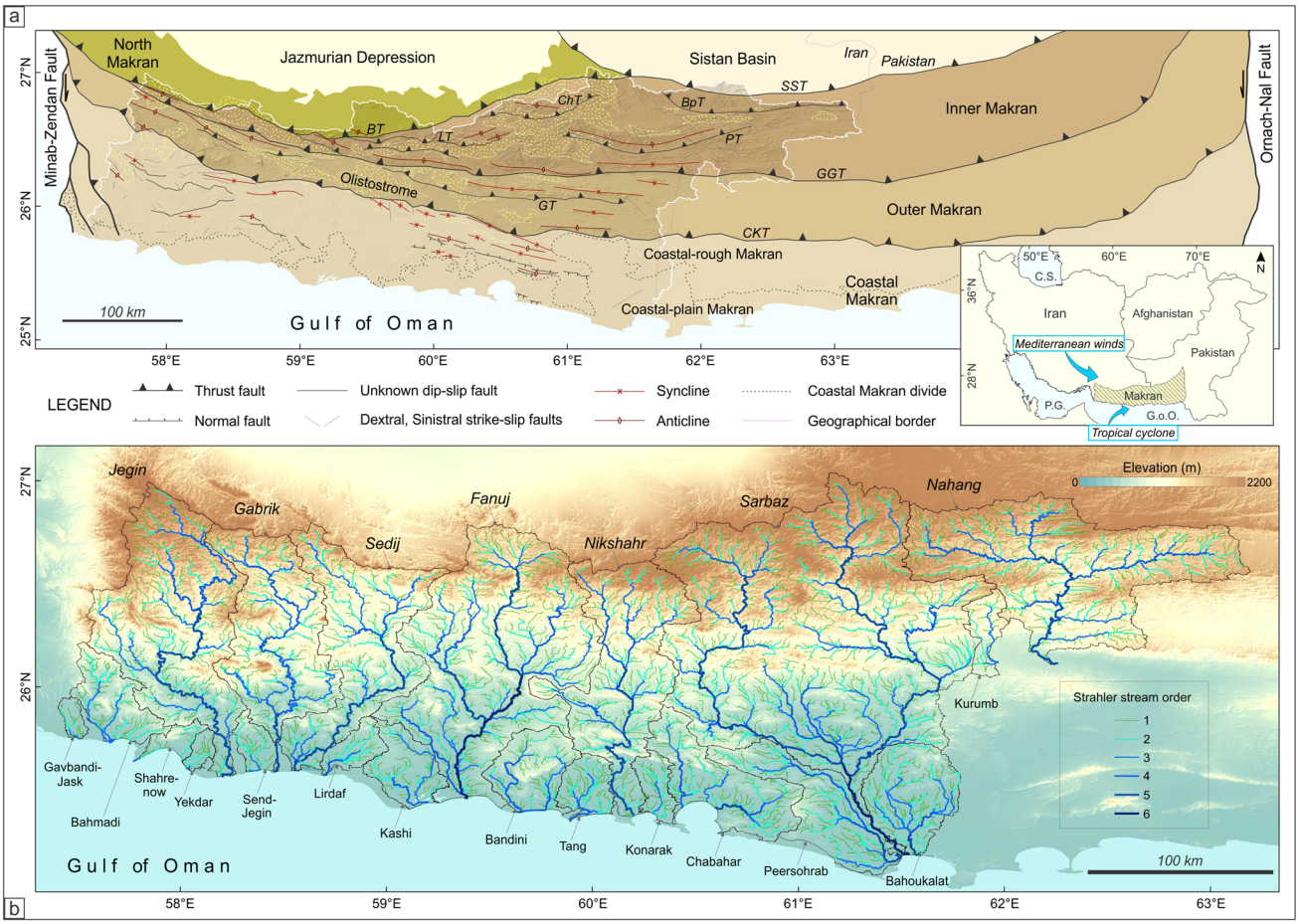

Fig. 1 **a** Simplified map of the Iranian onshore Makran with tecto-stratigraphic zones and major structures of the studied area (relief part with white boundary) based on Dolati (2010). Distribution of olistostromes (yellow polygons; Burg et al. 2008) modified with Google earth image. Abbreviations: *BT* Bashakerd Thrust, *SST* Sistan-Siahan Thrust, *BpT* Bamposht Thrust, *ChT* Chanf Thrust, *LT* Lashar Thrust, *PT* Pishamak Thrust, *GGT* Ghasr-e-Ghand Thrust, *GT* Gativan Thrust, and *CKT* Chah Khan Thrust. The blue arrows in inset Fig. 1a indicate dominant air masses from south and north, compiled from Fleitmann et al. (2007) and abbreviations: *C.S.* Caspian Sea, *P.G.* Persian Gulf, *G.o.O.* Gulf of Oman. **b** Topographic overview of the Iranian Makran main River Basins (similar area presented in Fig. 1a by white polygon and relief) with six color-coded Strahler orders from a TanDEM-X 12.5 m image (https://tandemx-science.dlr.de/). River catchments are represented by the local names and black polygons

have been distinguished in the offshore Makran based on their seismic character: oceanic crust mega-sequence, Himalayan turbidite mega-sequence, Makran sand mega-sequence, and growth mega-sequence (Minshull and White 1989; Kopp et al. 2000; Kukowski et al. 2001; Schluter et al. 2002; Grando and McClay 2007). Onshore Makran with heterogeneous structural and geomorphological patterns from east to west, and north to south is structurally subdivided into four main tectonostratigraphic zones. The main tectonostratigraphic zones from north to south that the river system drains are: the North Makran, the Inner Makran, the Outer Makran, and the Coastal Makran (Fig. 1a; e.g. Dolati 2010; Burg et al. 2013). In detail, major headwaters drain the North Makran, middle streams incise the Eocene to Miocene turbidites of the Inner and Outer Makran, and downstream parts flow over and flood the Late Miocene–Pliocene shallow marine (shelf and delta) deposits along the Coastal Makran during rainy seasons. From the Iranian Makran toward the Pakistani Makran, the river channels are deflected from the almost N-S flow direction to the E-W direction along the regional fault-related large elongated folds. Makran's western drainage pattern is relatively shorter than its eastern side and flows downslope of a steadily growing wedge (Haghipour and Burg 2014). Finally, all these rivers discharge into the Gulf of Oman (Fig. 1a, b).

Previous geomorphological analyses based on swath profile, longitudinal stream profile, and channel steepness index on the drainage systems of Iranian Makran, indicate that some rivers are in morphological disequilibrium (Haghipour and Burg 2014). According to Kober et al. (2013), the geomorphic evolution of the Iranian Makran has been controlled by the prevailing SW-Asian monsoon and Mediterranean winter rainfall and the regional surface uplift processes resulting from the Arabia–Eurasia convergence. Exposure ages (^{10}Be) from the alluvial river terraces (Haghipour et al. 2012) suggest that the active folding system is an adequate process to absorb much of the shortening amount and describe partly the lack of frequent seismicity (e.g. Heidarzadeh et al. 2008) of Makran. The remaining convergence may be absorbed by creep on associated blind décollements and thrust faults (Haghipour et al. 2012). On the other hand, seismological and geomorphological investigations across Makran (Penney et al. 2017), and field mapping, remote sensing, and dating (^{14}C, OSL, ^{230}Th/U) approaches of the uplifted marine terraces (Normand et al. 2019a), indicate that most likely the offshore megathrust behaviour in Makran or heterogeneous accumulation of deformation in the overriding subducting plate caused considerable deformation during the Late Quaternary in the easternmost boundary of Iranian Coastal Makran.

A few studies investigated the geomorphological characteristics of Makran in different aforementioned aspects (Snead 2002; Vita-Finzi 2002; Haghipour et al. 2012; Kober et al. 2013; Haghipour and Burg 2014, 2015; Normand et al. 2019a, b). However, drainage pattern development across the Makran is still poorly known. The drainage network pattern is changing from west to east and north to south onshore Makran, while the climate pattern is almost homogenous across the Makran (e.g. Kehl 2009). However, structural and geomorphological patterns of the onshore Makran Accretionary Wedge (e.g. Burg 2018) vary from the west (Iran) to east (Pakistan) and north to south for several reasons: Different convergence rates from west to east (e.g. Vernant et al. 2004; Penney et al. 2017), exposure of Makran ophiolite belt in the west (the North Makran zone; Hunziker et al. 2015), presence of regional-scale olistostrome (over 10,000 km^2 area with ~ 600 m thickness) in the west Makran (Burg et al. 2008), different deformation pattern of the western and eastern boundary of Makran due to the presence of Minab-Zendan and Ornach-Nal mega strike-slip faults (Fig. 1a) in the west and east Makran, respectively (e.g. Ellouz-Zimmermann et al. 2007; Grando and McClay 2007), and distinct uplift rate of the coastal terraces along the Makran coast (Normand et al. 2019a). Meanwhile, the Makran Accretionary Wedge, which is located in a regional compressional tectonic setting, locally behaves as an extensional system due to slab-rollback since the Late Miocene-Pliocene (e.g. Burg et al. 2013). In this case, the role of thrust faults and related folds (mostly in the Inner and Outer Makran) and normal faults (Coastal Makran) in drainage pattern development is unclear. In addition, the role of olistostrome as a cohesive sediment mass that covers partly the tectono-sedimentary structures is still unclear in the development of drainage patterns in the Iranian Makran. Taken together, these characteristics make the onshore Makran Accretionary Wedge an ideal case to investigate the simultaneous role of thrust faults and normal faults in drainage pattern evolution/development in a region with extremely dry climate settings and perfect rock exposure.

We present combined results from modern climate data, catchment-topographic metrics of 191 sub-catchments, and structural and field evidence to characterize the controlling factor(s) of drainage pattern evolution across the different tectono-stratigraphic zones of Iranian onshore Makran. To better understand the relationship between drainage patterns and fault systems as the main geological structures of the Makran Accretionary Wedge (e.g. Burg 2018; Normand et al. 2019a), we examined the impact of active faulting on river systems by using channel steepness index, topographic profiles, and field observations. Finally, the results were combined with the sediment connectivity index to identify the region(s) most vulnerable to erosion, sediment supply, and deposition.

Study area

The north-dipping subduction of the Arabian plate beneath the Eurasian plate formed Makran Accretionary Wedge in SE Iran (Iranian Makran) and SW Pakistan (Pakistani Makran, Fig. 1a inset). The subduction started in the Late Cretaceous (e.g. McCall 2002; Alavi 2007) and is still active (~ 2 cm/yr; e.g. Masson et al. 2007). The onshore Makran "with ~ 200 km width" is limited to the Jazmurian (Iran) and Mashkel (Pakistan) depressions in the north and the Gulf of Oman in the south (Burg 2018). The offshore Makran, with ~ 150 km wide in the north of the Gulf of Oman, formed the seaward margin of the onshore Makran (White 1982). From west to east Makran, this wedge is stretched ~ 1000 km between the Minab-Zendan and Ornach-Nal strike-slip faults, respectively (Fig. 1a; McCall 1997). In the frame of this study, we focus on the Iranian onshore Makran.

The Iranian onshore Makran includes four main tectono-stratigraphic units from north to south: North, Inner, Outer, and Coastal Makran (Figs. 1a and 2; Burg 2018). The zones are separated by the presence of almost W-E striking thrust faults. The Inner and Outer Makran are separated by the Ghasr-e-Ghand Thrust (GGT), whereas the Outer Makran is separated by the Chah Khan Thrust (CKT) from the Coastal Makran (Figs. 1a and 2). Both the Inner and Outer Makran pinched out to the west, and reaching their maximum extension in the Pakistani Makran, while the Coastal Makran reaches its maximum extension in the west of Iranian Makran (Fig. 1a). Presence of several small thrust faults with west–east strike within the Inner and Outer Makran indicates dominant fault-related internal deformation pattern in these zones (Dolati 2010). The northern boundary of Inner Makran corresponds to the Sistan-Siahan Thrust (SST), which separates Makran from the south Sistan Basin Eocene deep marine turbidites (Mohammadi 2016b; Fig. 1a). The presence of North Makran in our study area is negligible (Fig. 1a). Lithologically, Inner and Outer Makran consist of over 7 km deep-marine turbiditic sandstone and shale intervals, and Coastal Makran is dominantly composed of deep to shallow marine and deltaic sandstones and marls (Fig. 1a; Mohammadi 2010; Mohammadi et al. 2016a, 2017; Kaveh et al. 2020). To better understand the different structural and geomorphological controlling processes on the drainage pattern development, we divided the tectono-stratigraphic Coastal Makran zone into two geomorphological zones: Coastal-rough Makran with high relief in the north, and Coastal-plain with low topography in the south (Fig. 1a). The Coastal-plain exhibits different northward and lateral extension from west to east Makran, with its maximum growth in the southeasternmost of Iranian Makran (Sarbaz Catchment; Fig. 1b), which is consistent with the maximum uplift rate of coastal terraces (Haghipour et al. 2012; Normand et al. 2019a). The surface uplift rates for the Coastal-plain terraces mostly range between 0.05 and 1.2 mm/year, except an anomalous high rate about 3–5 mm/year in the east (Normand et al. 2019a). Compared to other subduction zones around the world, these rates are high, indicating the upper plate has been accumulating considerable permanent deformation during the Late Quaternary. However, the fact that short-term (Holocene) and long-term (Pleistocene) uplift trends are different may indicate that large, infrequent earthquakes strongly influenced the short-term uplift trends in the region (Normand et al. 2019a, b).

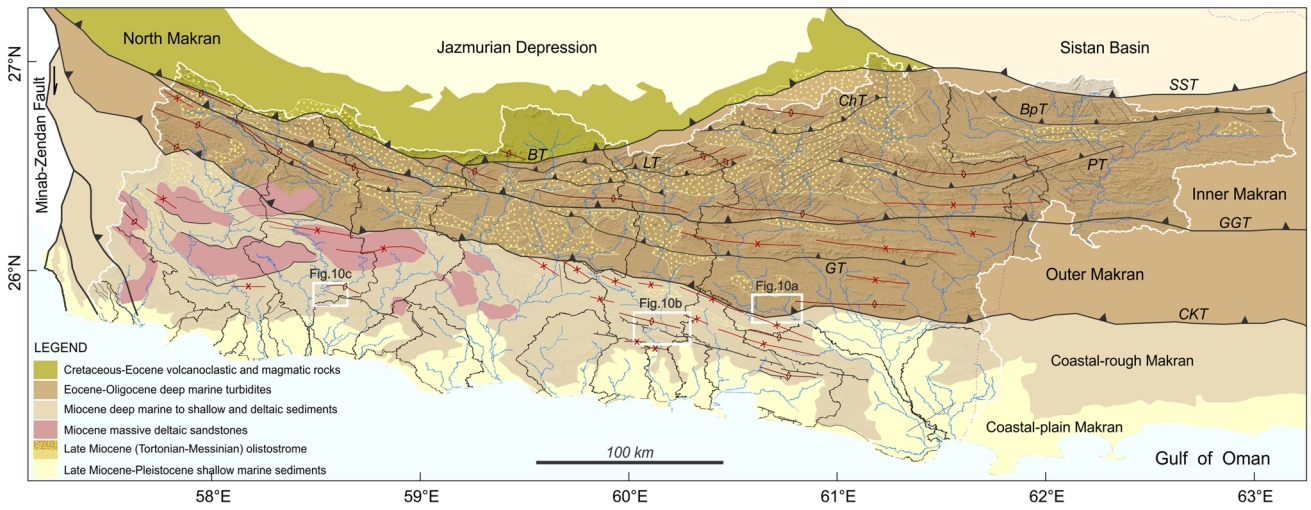

Fig. 2 A combined overview of the geological map and main drainage system in the onshore Iranian Makran (our study area). Lines and river catchments as in Fig. 1a, b

Fault systems in onshore Makran are primarily characterized by several thrust faults, particularly in the Inner and Outer Makran. These faults with the nearly west–east strike correspond to the Makran main tectono-stratigraphic unit boundaries (Fig. 1a). The thrust faults are Eocene to Early Miocene in age in onshore Makran with gradually younging trend toward the south. They formed by the ongoing accretion of deep marine sediments due to the northward subduction of the Arabian Plate beneath the Central Iran and Afghan blocks (Burg 2018). Normal faults are relatively young and cut out the Late Miocene–Pleistocene sedimentary rocks and uplifted terraces of the Coastal Makran (Fig. 1a; e.g. Normand et al. 2019a). Several strike-slip faults with different strikes exist across the Makran, especially toward the east, displaying up to 100 m displacements of the older geological structures and geomorphological features on satellite images (e.g. Dolati and Burg 2013). A number of conjugate strike-slip faults (dominant NW–SE dextral and NE-SW sinistral) are scattered in onshore Makran, cutting the older thrust faults, folds, the Eocene–Miocene rocks in the Inner and Outer Makran, and Pliocene to Pleistocene sedimentary rocks in the Coastal Makran (Fig. 2). According to Dolati and Burg (2013), the conjugate strike-slip faults suggest bulk NNE–SSW shortening in onshore Makran. The fold systems are distributed across the region. They are mainly tight folds in the Inner Makran, while toward the Outer and Coastal Makran change to gentler folds (Burg 2018). These folds are not continuously exposed throughout the Iranian Makran, and some parts are buried by olistostrome (Fig. 1a; Burg et al. 2008). The olistostrome represents massive mass flow on a regional scale caused by paleotsunami in the Late Miocene (Tortonian-Messinian; Burg et al. 2008). The recorded instrumental seismicity is sparse in the Iranian onshore Makran and no large-magnitude event is documented (e.g. Byrne et al. 1992; Rajendran et al. 2013; Penney et al. 2017). However, the great instrumental earthquake reported from 1945 (Mw = 8.1; Ambraseys and Melville 1982) Offshore Pakistani Makran caused a tsunami (Hoffmann et al. 2013), significantly affecting the Iranian Makran indicating that the Makran offshore is a seismically active area (e.g. Musson 2009).

The main drainage systems of the Iranian onshore Makran are classified into two main groups based on drainage area. The first group includes major river basins with areas varying between ~ 4500 km^2 and ~ 17,500 km^2, known as Jegin, Gabrik, Sedij, Fanuj, Nikshahr, Sarbaz, and Nahang from west to east of Iranian Makran (Fig. 1b; Table S1). This headwater group is located mainly in the Inner Makran at elevations ~ 1200 to ~ 2200 m and flows through the Outer and Coastal zones (Figs. 1 and 2). The second group contains small rivers with a catchment area between 200 km^2 and ~ 2700 km^2 (Fig. 1b; Table S1). This group drains from the Coastal-rough Makran at elevations ~ 200 to ~ 1400 m (Fig. 1b). The trunk channel of both groups flows from north to south and discharges to the Gulf of Oman. The Sarbaz and Nahang Rivers are the only perennial rivers, and all the other Iranian Makran rivers are ephemeral (Fig. 1b; Haghipour and Burg 2014).

The Makran climate pattern is divided into humid Early Holocene until 6500 years B.P. (Fleitmann et al. 2007), relatively arid during Late Holocene (Cullen et al. 2000; He et al. 2020), and arid/semi-arid in present day (e.g. Kehl 2009; Bourget et al. 2010) with poor vegetation cover (Miller et al. 2016). The precipitation type is generally characterized by a Mediterranean-type humid climate, which mostly affects the Inner and Outer Makran with intense rainfalls during autumn and winter. In contrast, the Indian dry monsoons and rarely the tropical cyclones affect the Makran in the summer (Fig. 1a inset; e.g. Weyhenmeyer et al. 2002). The storm Gonu, which occurred on June 2007, is an example of a tropical cyclone that affected also the Iranian Makran region (e.g. Fritz et al. 2010).

The Coastal-plain Makran is also subject to tidal oscillations, which is dominated by meso-tidal in the Gulf of Oman (1.8–3 m; Shah-Hosseini et al. 2018). The maximum wave height (~ 3 m) was recorded in the Chabahar coast with SSE–NNW direction, particularly from January to June in agreement with the south-eastern Indian summer monsoon (Shah-Hosseini et al. 2018).

Data and methods

Time series analysis on modern precipitation data

To reveal the spatial and temporal characteristics of modern precipitation patterns in the Iranian Makran, we used 43 years (October 1972 to September 2017, data from 2017 until now is not available) daily rainfall dataset from 43 gauging meteorological stations. Based on time period coverage (43 years) and the geographical locations of 69 available stations, 43 stations were selected to have a homogenous distribution pattern (Fig. S1). From the selected stations, we calculated mean areal precipitation (Fig. 3a), long-term mean annual precipitation (Fig. 3b), monthly mean precipitation with extreme values (Fig. 3c), and trend analysis (Fig. S2).The linear regression analysis was performed to determine Annual Maximum rainfall (AMAX; Dales and Reed 1989) for each station (Fig. S2). In addition, a spatial interpolation method was used in ArcGIS application to create a surface map of long-term mean annual rainfall across the onshore Iranian Makran (Fig. 3c).

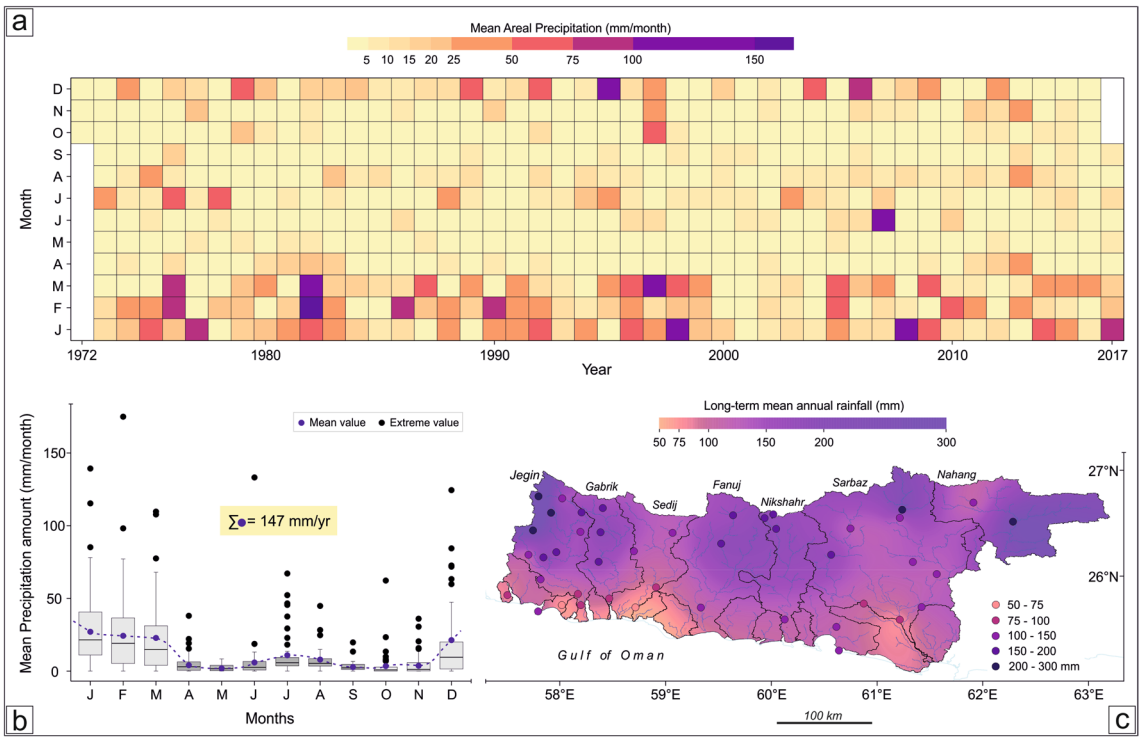

Fig. 3 Modern climate pattern across the Iranian Makran. **a** Monthly values of mean areal precipitation in the study area between 1972 and 2017 period, **b** Box-and-whisker plots of mean monthly precipitation values with calculated mean annual precipitation displayed in the yellow rectangle, **c** Long-term mean annual precipitation in the onshore Iranian Makran based on meteorological stations (color-coded circles on the top). Interpolation method is used to create this background. Names as in Fig. 1b

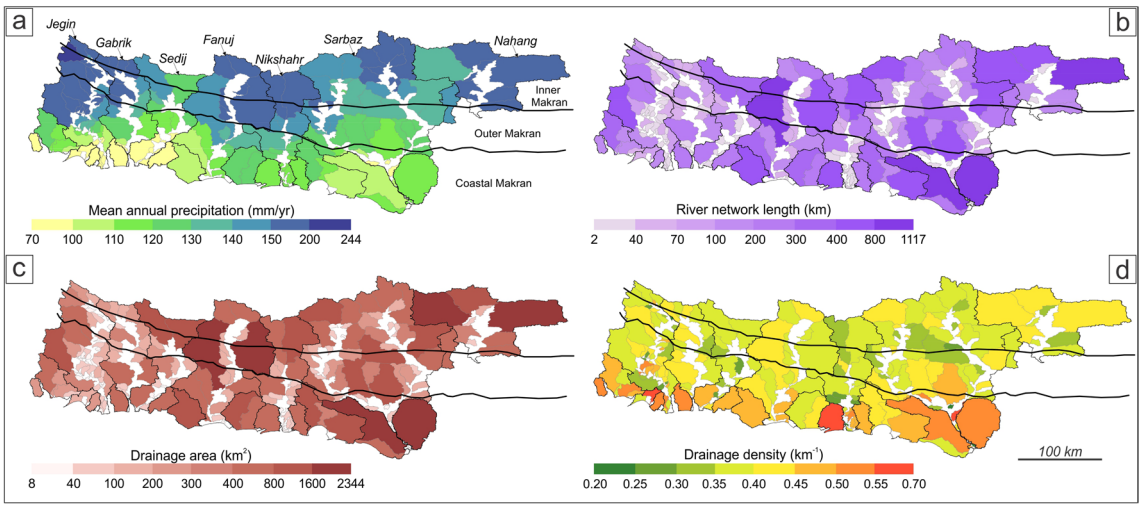

Fig. 4 The precipitation and catchment metrics extracted from meteorological data and TanDEM-X 12.5 m, respectively, for 191 subcatchments of the study area: **a** Mean annual precipitation, **b** River network length, **c** Drainage area, and **d** Drainage density. The lines display divide between Makran tectono-stratigraphic zones (black lines)

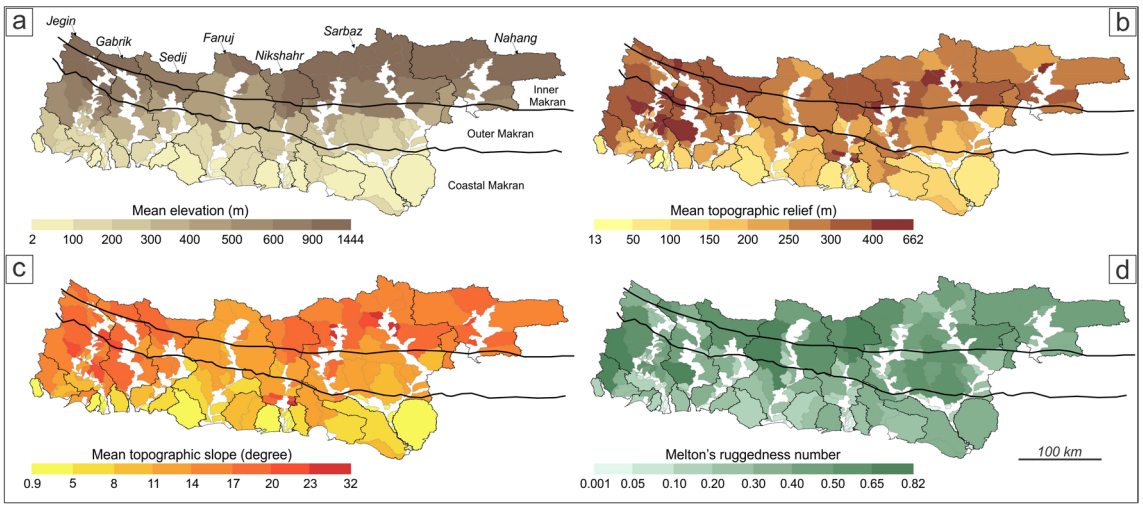

Fig. 5 Topographic parameters derived from TanDEM-X 12.5 m: **a** Mean elevation, **b** Mean topographic relief, **c** Mean hillslope angle, and **d** Melton's ruggedness number. The solid lines as Fig. 4

Topographic analyses based on TanDEM-X

Catchment-topographic metrics, regression analysis

To find out the geomorphic pattern differences across the Makran zones, we use ArcGIS to perform terrain analysis including catchment parameters and topographic metrics calculations (Figs. 4a–d and 5a–d; Table S1). To provide another perspective on Makran drainage pattern variations in detail, we chose these methods, while avoiding repetition of previously used methods (e.g. Haghipour and Burg 2014), to make a multi-proxy data set to shed light on the river catchment development in the poorly understood Onshore Makran. Our catchment-topographic analysis were extracted from the TanDEM-X images with a spatial resolution of 12.5 m, launched between 2010 and 2014 (https://tandemx-science.dlr.de/). The performance of TanDEM-X is quite well across the semi-arid to arid regions due to sparse or no vegetation cover (Wessel et al. 2018), like Makran. Based on these images, we classified the Iranian Makran river networks into the six Strahler stream order, containing 7130 river segments (Fig. 1b). Some characteristics of rivers can be inferred by stream order, specifically drainage pattern types. Drainage pattern type mainly depends on geological structures, lithology erodibility of rocks, and climate setting. Hence, this can be used as a proxy to show the controlling factor(s) of surface dynamics and active tectonic (e.g. Keller 1986; Twidale 2004; Bull 2011). To do a precise comparison between three main zones of Iranian Makran, we extracted 191 sub-catchments from third-order and second-order (in case of a lack of third-order) of the drainage network, including 49, 39, and 103 sub-catchments from the Inner, Outer, and Coastal Makran, respectively (Figs. 1a and S3). As a regional-scale work, the mentioned Strahler orders are large enough to show the topographic-climatic variations across the onshore Iranian Makran. The North Makran is excluded from our work due to a negligible presence in our study area (Fig. 1a). Catchment parameters such as river network length, drainage area, and drainage density were calculated for mentioned sub-catchments (Fig. 4b–d; Table S1). Drainage density is a total river length per drainage area, and indicates the degree of fluvial dissection (e.g. Horton 1932, 1945). In addition, topographic metrics including elevation, relief, slope angle, Melton's ruggedness number were also calculated, and all were presented in mean values (Fig. 5a–d; Table S1). A summary of catchment parameters and topographic metrics equations is presented in Table 1. Relief is an essential metric to understand the topography of a region and is in good agreement with the slope angle (Montgomery and Brandon 2002; DiBiase et al. 2010). Melton's ruggedness is also one of the important indices, which can clarify more characteristics of topographic relief. This index is characterized by steepness and length of the slope to indicate the instability of the land surface, topographic roughness, and structural complexity (Strahler 1957; Melton 1958; Wilford et al. 2004). High Melton's ruggedness number correspond to regions with steeper slope and rough relief, which may be the consequence of tectonic uplift, while low values usually indicate tectonic stability or minimal uplift (Valkanou et al. 2020). In addition, this metric allows us to identify the regions that have experienced sediment production and transportation due primarily to bedrock incision and erosion (Wilford et al. 2004). In all mentioned metrics, the lithological effect is considerable.

Table 1 Description of GIS-based catchment-topographic metrics derived from TanDEM-X 12.5 m

Aspect	Catchment Parameters	Abbr.	Unit	Description	Reference
Linear	Stream order	So	–	Hierarchical rank, Strahler method	Strahler (1964)
	River network length	L	km	Lr = L1 + L2.... + L6	Horton (1945)
	Drainage area	A	km^2	Area draining to catchment outlet	Schumm (1956)
Areal	Drainage density	Dd	Km^{-1}	Dd = ΣLr/A	Horton (1932)
Topography	*Topographic metrics*				
	Elevation	Elev	m	Height above sea level	Moore et al. 1991; Wilson 2018
	Catchment Relief	CR	m	$CR = Elev_{max} - Elev_{min}$	
	Hillslope angle	S	°	The degree of inclination of a feature relative to the horizontal plane	
	Melton's ruggedness number	Mrn	–	Mrn = CR * Dd	Melton 1965
	Sediment connectivity index	IC	–	The degree of linkage that controls sediment fluxes throughout landscape	Borselli et al. 2008; Crema and Cavalli 2018

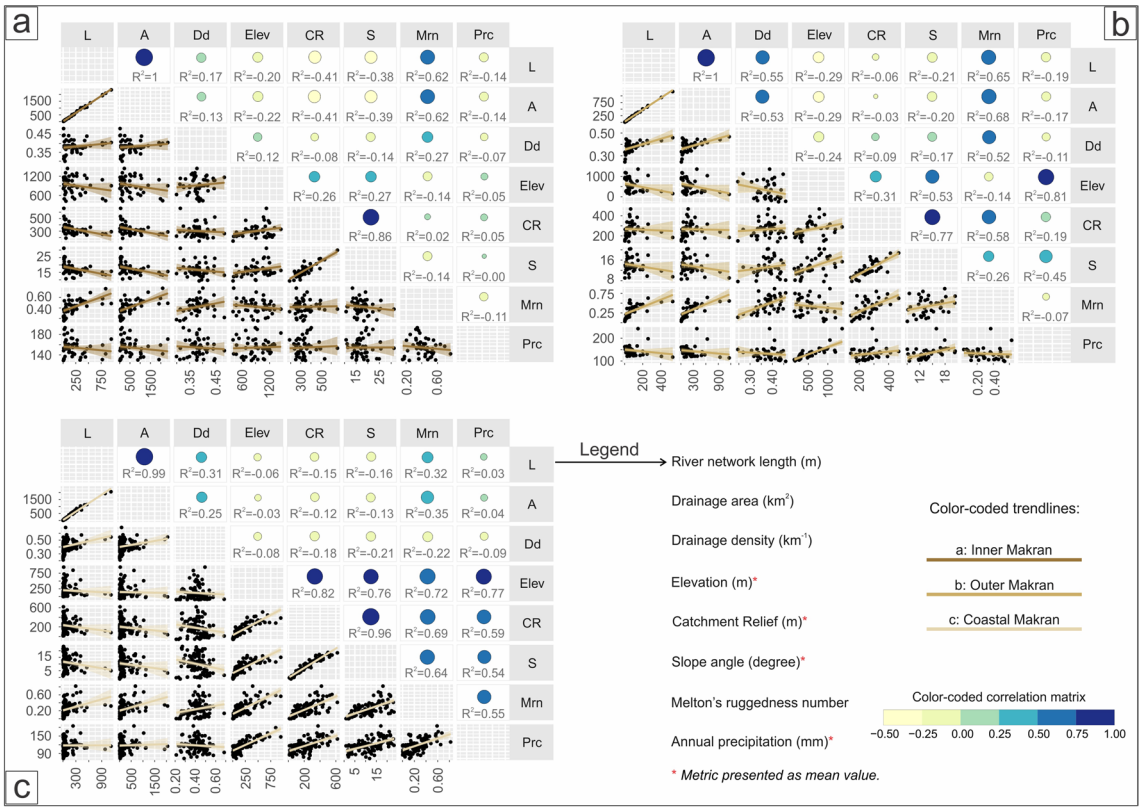

Fig. 6 Correlation matrix of climatic-catchment-topographic variables selected to distinguish their relationships in Makran different tectono-stratigraphic zones: **a** Inner Makran, **b** Outer Makran, and **c** Coastal Makran

The catchment parameters and topographic indices are separately calculated for each of the 191 sub-catchments (Figs. 4 and 5) and the results are summarized in Table S1 separately for each zone.

To better understand and assess possible controls on drainage pattern evolution, the relationship between calculated catchment parameters and topographic-climatic metrics, linear regression analysis was conducted separately for each studied zone (Fig. 6a–c). Additionally, topographic variations across distinct zones were investigated during several field works (Fig. 7a–k), and using high resolution satellite images (Fig. 7l–n).

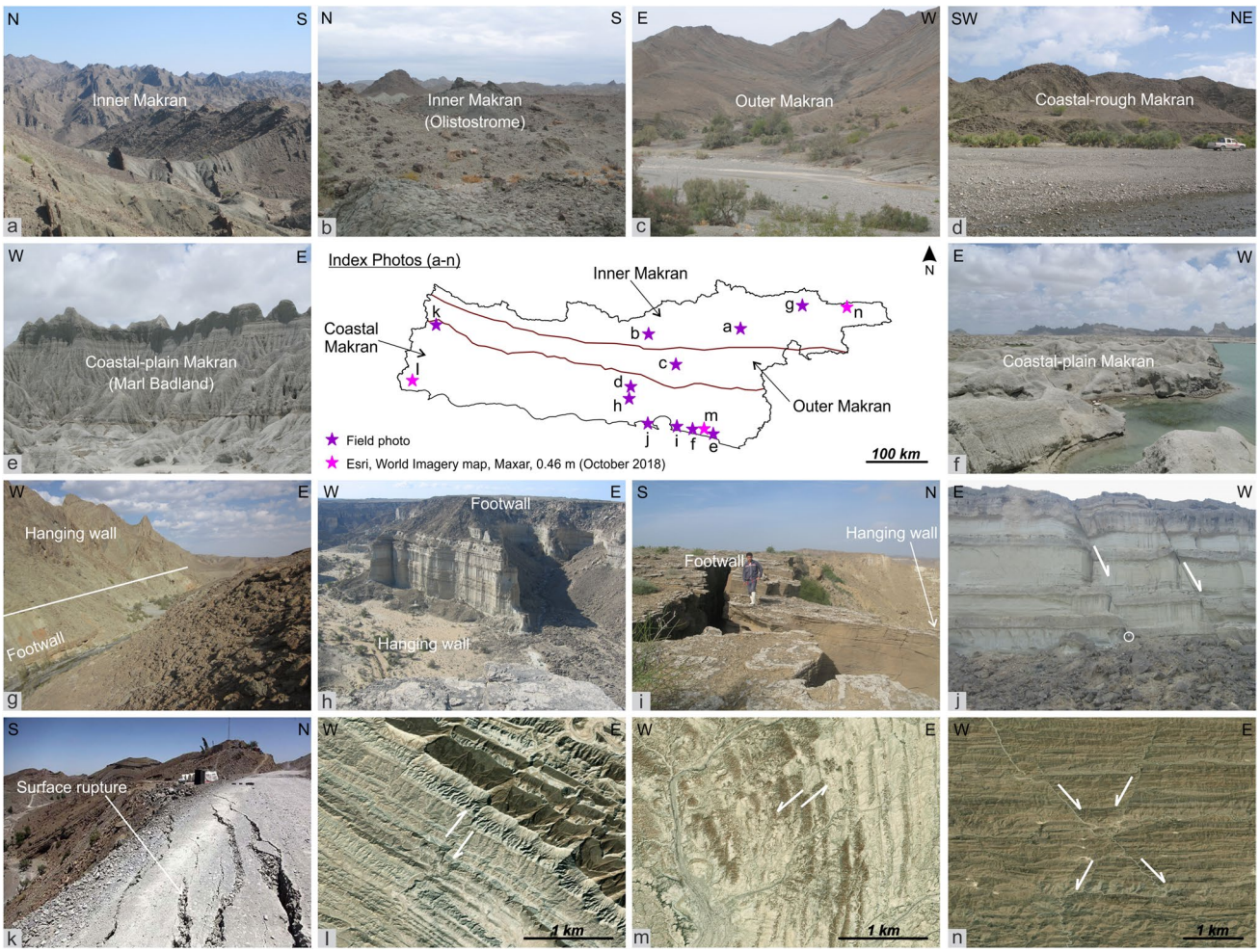

Fig. 7 Field evidence showing the different topographic overview of the Iranian Makran tectono-stratigraphic zones: **a** Inner Makran, **b** Olistostrome distribution in Inner Makran, **c** Outer Makran, **d** Coastal-rough Makran, **e** Badlands in Coastal-plain Makran, **f** erosional surface of Coastal-plain Makran, **g** thrust faulting (white line, Bamposht Thrust), **h**, **i**, **j** the Late Quaternary normal faulting on the Coastal-rough (**h**) and uplifted coastal terrace (**i**, **j**), **k** surface rupture due to strike-slip faulting (Irar earthquake, 11 May 2013; photo by Geological Survey of Iran), **l**, **m**, **n** some evidence from strike-slip faults on the satellite image (Esri, world imagery base map, Maxar, 0.46 m resolution) in the western and eastern part of Coastal-plain Makran (**l** and **m**, respectively), and conjugate strike-slip fault in the eastern part of Inner Makran (**n**). The location of all photos (**a**–**n**) is shown in the index

Channel steepness index and valley width to depth ratio

The channel steepness index, k_s, is a property of rivers, which can encode information about erosion rates, lithology, and uplift (e.g. Whipple and Tucker 1999; Gailleton et al. 2021; Smith et al. 2022), and is widely used in tectonic geomorphology because its empirical correlation with erosion rates is positive (e.g. Cyr et al. 2010; DiBiase et al. 2010; Kirby and Whipple 2012; Scherler et al. 2014; Haghipour and Burg 2014; Mandal et al. 2015; Harel et al. 2016; Kaveh Firouz 2018; Peri et al. 2022). In fact, k_s is a metric derived from the stream power model. A power law relationship between channel gradient and drainage area was noted by Morisawa (1962), which led to a means of normalizing river gradients. These observations was formalized into the slope–area relationship with a concavity index (θ), which describes how quickly river gradient decreases with increasing drainage area (Flint 1974), and k_s that describes the relative steepness of a river regardless of its drainage area:

$$S = k_s A^{-\theta} \tag{1}$$

where S is the channel slope ($S = dz/dx$, z is the elevation and x the flow distance); and A is the drainage area. To compare k_s within different channels, the steepness index is typically calculated with a fixed value of θ. This is called the reference concavity index, denoted by θ_{ref}. Using a reference concavity index, the channel steepness index is normalized, and is denoted with the symbol k_{sn} (Wobus et al. 2006). Despite the importance of constraining θ for calculating the channel

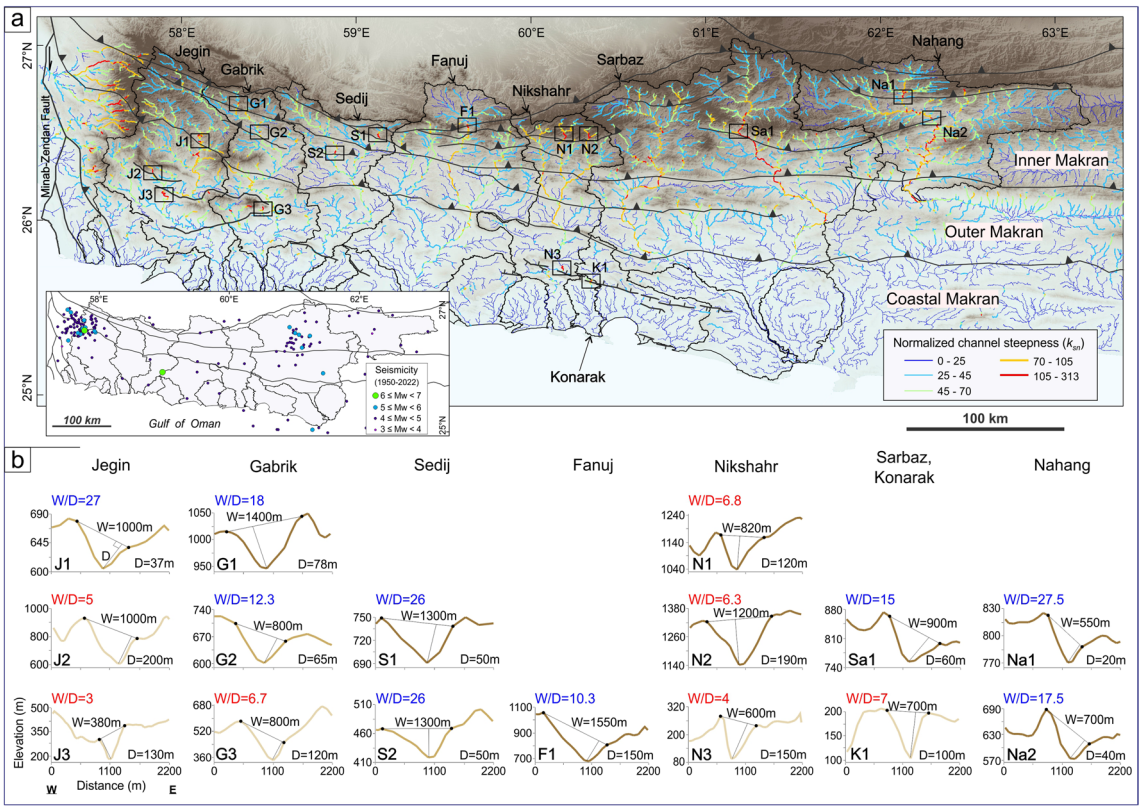

Fig. 8 **a** The normalized channel steepness (k_{sn}) map of Iranian Makran on TanDEM-X 12.5 m. The black polygons represent the main river catchments. The brown and purple lines are thrust and normal faults (names as in Fig. 1a), respectively. The small black rectangles indicate the locations of profiles shown in Fig. 8b. The inset Fig. 8a displays Instrumental seismicity of Iranian Makran (1950–2022). **b** The topographic profiles extracted from DEM, the color-coded profiles as shown in Fig. 6 separated for each zone of Makran. The W and D parameters are width of incision at surface and depth of incision, respectively. The W/D ratio is classified to > 10 (blue letters) and < 10 (red letters)

steepness index, it is often assumed that $0.4 < \theta < 0.6$ (e.g. Kirby and Whipple 2012; Tucker and Whipple 2002; Whipple 2004), typically a value of 0.45 (Gailleton et al. 2021).

A normalized channel steepness (k_{sn}) map has been generated using the digital elevation models (DEMs), Topotoolbox-2 (Schwanghart and Scherler 2014, 2017) and related codes from Gallen and Wegmann (2017) for the entire Iranian Makran (Fig. 8a). To create this map, we selected a set "threshold drainage area" of 10^7 m^2, "concavity index" of 0.45, "smoothing distance" of 1000 m, and "an arbitrary scaling area" of 1 m^2 (e.g. Snyder et al. 2000; Wobus et al. 2006). These values were derived from Haghipour and Burg (2014), as well as considering the Strahler order used in our study. The k_{sn} values for Makran river system are categorized into five colour-code lines. The red colour shows highest values (> 105), while blue colour indicates the lowest (< 25; Fig. 8a). The k_{sn} is one of the significant topographic metrics in tectonic geomorphology and can be used as a proxy for uplift, erosion and incision (e.g. Kirby and Whipple 2012).

To detect the river incision stage across the Iranian Makran, we extracted 16 topographic profiles normal to the main rivers (Fig. 8b) with the highest k_{sn} value, which are mostly located on the fault zones (Fig. 8a). In fact, the channel incision dimensions (2D) were measured from the profiles to determine whether fault systems and channel incisions are related (e.g. Beechie et al. 2008). Therefore, we measured the incision width at surface (W) and depth (D) from aforementioned profiles, as well as the W/D ratio to determine most recent activities of faults, where the seismicity is sparse.

Sediment connectivity index

We also tested the sediment connectivity index (IC) in relation to the degree of which river system coupling with the transport of water and sediment flux (Figs. 1b and 9a). This index is defined as the degree of coupling between sediment sources and sinks in a system and identifies how efficiently sediment is transported from hillslopes to

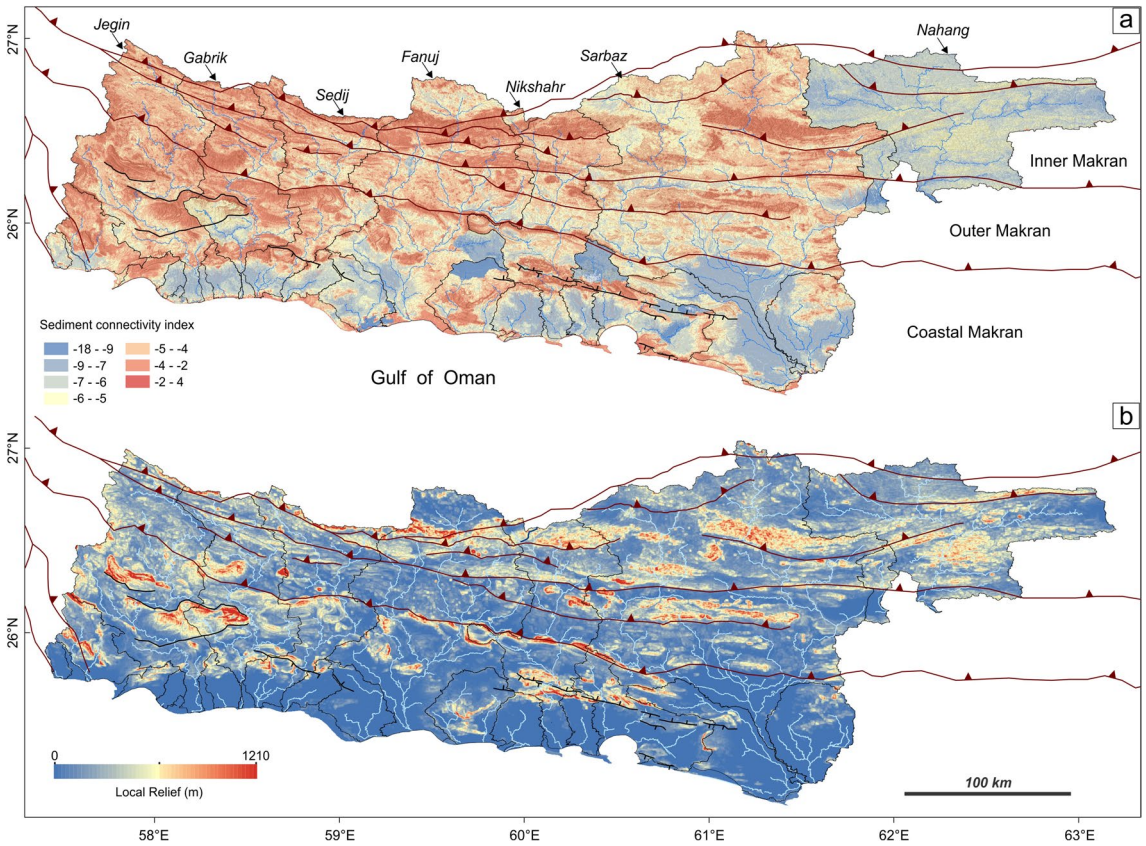

Fig. 9 **a** Pattern of sediment connectivity index (a proxy for erosion hazard susceptibility) throughout the Iranian Makran river catchments. **b** Local relief map with a 2 km radius sampling window over the region. Lines and names as Figs. 1 and 2

channels and within channels (Cavalli et al. 2013). This measurement provides overall information about sediment connectivity patterns in the catchment. The low values show a sediment trap and depositional pattern, while high values are indicative of an erosional pattern (e.g. Borselli et al. 2008; Cavalli et al. 2013; Bracken et al. 2015; Zingaro et al. 2019). Understanding of sediment transfer that is responsive to tectonic activities and base-level changes can provide valuable insight into erosional responses of topography and mass-wasting dynamics. To obtain a comprehensive view of erosional/depositional patterns in the Iranian Makran, sediment connectivity analysis was performed at the main catchment scale (Fig. 9a).

The connectivity index has been implemented through the Model Builder application running in ArcGIS 10.6.1 (ESRI 2018), and it uses functionalities and algorithms available in the Spatial Analyst extension and TauDEM 5.3.7 tool (https://hydrology.usu.edu/taudem/taudem5/index.html). IC is derived following the approach of Borselli et al. (2008), who defined the Index of Connectivity as:

$$IC = \log_{10}\left(\frac{D_{up}}{D_{dn}}\right) \tag{2}$$

where the upslope and downslope components of connectivity are D_{up} and D_{dn}, respectively. IC was defined in the range of $(-\infty, +\infty)$, with connectivity increasing for larger IC values.

The D_{up} is the potential for downward routing of the sediment produced upslope and is estimated as follows:

$$D_{up} = \overline{WS}\sqrt{A} \tag{3}$$

where $\overline{W}$ is the mean weighting factor of the upslope contributing area, $\overline{S}$ is the mean slope gradient of the upslope contributing area (m/m) and A is the upslope contributing area (m^2).

The downslope component D_{dn} estimate the flow path length that a particle has to travel to arrive to the nearest target or sink. Thus, D_{dn} can be calculated as:

$$D_{dn} = \sum_i \frac{d_i}{W_i S_i} \quad (4)$$

where d_i is the length of the flow path along the i^{th} cell according to the steepest downslope direction (m), W_i and S_i are the weighting factor and the slope gradient of the i^{th} cell, respectively. It is important to note that d_i can assume two values: cell size (l) in the case of cardinal direction and $l\sqrt{2}$ in the case of diagonal direction.

Results

Precipitation gradients

Based on local meteorological data, mean areal precipitation presented on a heat-map (Fig. 3a), reveals an arid climate pattern across the Iranian Makran. The Inner and Outer Makran recorded relatively higher amounts of long-term (43 years) annual precipitation (130–193 mm and 117–242 mm, respectively) compared to the Coastal Makran (72–184 mm; Fig. 4a). According to the box and whisker plot, the monthly distribution of precipitation shows most of the precipitations occur during December to March with several rainstorms (Fig. 3b). The spring and summer seasons are rather dry across the Makran. However, tropical cyclones (e.g. Gonu tropical cyclone in June 2007, Fritz et al. 2010) rarely occur in summer and affect the Makran and adjacent regions (Fig. 3a, b). Based on our large long-term data set (43 years), the mean annual precipitation is about 147 mm for the Iranian Makran, indicating an arid climate pattern for the region (Fig. 3b).

Linear regression analysis and long-term mean annual rainfall values indicate that the possibility of large storms (> 150 mm precipitation in short time) is not concentrated in the specific part of Makran. However, the Inner and Outer Makran are more capable of experiencing intense rainfall (100–150 mm) than the Coastal Makran (Fig. 3c).

Catchment-topographic metrics

Six Strahler stream orders display drainage pattern is mostly dendritic type across the Iranian Makran, except trellis type in the eastern limit of Inner and Outer Iranian Makran (Fig. 1b). There is no unique pattern of river network length relative to Iranian Makran zones from north to south and west to east (Fig. 4b). Most of the long river tributaries (> 600 m) are located in Fanuj, Sarbaz, and Iranian part of Nahang Catchments (Figs. 1b and 4b). Furthermore, the Peersohrab and Bahoukalat Catchments along the Coastal Makran show a high river network length. The drainage area displays an almost similar pattern to the river length (Fig. 4c). Drainage density is slightly higher (~ 1 km^{-1}) in the Coastal Makran compared to the Inner and Outer Makran (Fig. 4d).

The mean elevation, relief, and slope decrease from the Inner Makran to the Coastal Makran. There are some local exceptions (e.g. middle Nikshahr, middle Sarbaz, and upper Nahang catchments; Fig. 1b). However, Fanuj Catchment is significant, which shows lower topographic metrics than its western and eastern catchments (Fig. 5). Overall, a maximum mean elevation of 1444 m, the highest relief at ~ 660 m, and slope ~ 32° were observed in Inner Makran. These values are scattered throughout our study area (Fig. 5a–c). The Melton's ruggedness number varies between 0.001 and 0.82 in Iranian Makran (Fig. 5d) with maximum values (0.40–0.82) in the Inner and Outer Makran. While the low values (< 0.40) are dominantly scattered across the Coastal Makran (Fig. 5d). However, the lower Sarbaz Catchment is an exception, where the river and tributaries are tilted (Fig. 1b).

The Jegin and Gabrik River Catchments are considered separately from the other studied river catchments due to the high topographic values through their catchments (Figs. 4 and 5; Table S1). The high topographic values in the aforementioned rivers could be attributed to the Minab-Zendan Fault system activity (Fig. 1a) and exposure of massive deltaic sandstones (Fig. 2).

Our correlation analyses of catchment parameters, topographic metrics, and precipitation amounts revealed both positive and negative (inverse) correlations between these variables over three distinct zones of Iranian Makran. The correlation values are classified to very weak inverse (−0.50 to −0.25), weak inverse (−0.25 to 0), very weak positive (0–0.25), weak positive (0.25–0.50), moderate positive (0.50–0.75), and strong positive (0.75–1). They are shown as a color-coded matrix in Fig. 6. The relationships between catchment parameters and topographic metrics are very weak to weak inverse in all three zones of Iranian Makran. There are some exceptions with a very weak positive correlation. Melton's ruggedness is the only topographic metric that shows a moderate-strong positive correlation with catchment parameters in all three zones, except with drainage density in the Coastal Makran (Fig. 6). The relationships between topographic metrics (elevation, catchment relief, and Melton's ruggedness) are mostly weak inverse in the Inner Makran, weak-moderate in the Outer Makran, and strong in the Coastal Makran. The relief and slope angle are the only two metrics showing a strong positive correlation in all three zones. The correlation between precipitation amount and catchment parameters is mainly weak inverse for the entire Iranian Makran (Fig. 6). In contrast, the relationships between precipitation amount and topographic metrics are more positive in the Makran. A strong correlation was found between precipitation and elevation, which is strong in the Outer and Coastal Makran zones. This does not

apply to the Inner Makran since it has very weak positive/negative correlations (Fig. 6). These correlations suggest that the catchment parameters are not dominantly governed by topography or precipitation, and, instead, the other factors cooperate to control drainage patterns and landscape evolution.

Channel steepness response to active fault systems

The pattern of normalized channel steepness index (Fig. 8a) shows that the rivers draining the high relief of the Inner Makran have k_{sn} values between 45 and 300 $m^{0.9}$ that are well distributed from west to east Makran. Similar range of k_{sn} was observed for the Outer Makran, but mostly localized in the western part (Jegin and Gabrik Catchments). The k_{sn} values are mainly < 45 $m^{0.9}$ across the Coastal Makran, however, there are some local exceptions in the lower catchments of Jegin, Gabrik, Nikshahr, and Konarak rivers (Fig. 8a) with abrupt changes in k_{sn} values. Our mean topographic profiles on the regions with highest k_{sn} value (red colour-code mostly along trunk channels, Fig. 8a) show that the W (width of incision at surface) parameter is mostly higher than 1000 m in the Inner and Outer Makran, while it decreases to less than 1000 m in the Coastal-rough Makran (Fig. 8b). This is consistent with the U-shaped valleys in the Inner and Outer Makran, and V-shaped valleys in the Coastal-rough Makran, the old and young stages of incision, respectively. The D parameter (depth of incision) does not show a special trend across the zones, thus we consider the ratio between W and D (W/D) for each profile. This ratio is classified into > 10 and < 10 (Fig. 8b). All the profiles in the Inner and Outer Makran zones exhibit W/D ratio > 10, except profiles N1, N2 in the Nikshahr Catchment. These two profiles are located on the hanging wall of the Lashar Thrust (Figs. 1a and 8a), while the footwall is covered by more erodible olistostrome (Fig. 1a). All the profiles in the Coastal-rough Makran indicate V-shaped valleys with W/D ratio < 10, in concordance with presence of almost W–E striking normal faults (the lower and upper catchment of Nikshahr and Konarak, respectively; profiles N3, and K1; Fig. 8) and unknown dip-slip faults (the middle and lower catchment of Jegin and Gabrik, respectively; profiles J2, J3, and G3, Fig. 8). This evidence suggests the possible activities of normal faults, where they cut the Pliocene sedimentary rocks (Fig. 7j).

Sediment connectivity index

Sediment connectivity results are displayed in a map, with values ranging from low (−18 to −6, blue colour spectrum), neutral (−6 to −5, cream colour), to high (−5 to 4, red colour spectrum, Fig. 9a). Most of the high values appear in areas with high topographic relief and slope. However, there are some regions with high topographic metrics (i.e. southern part of Nahang Catchment) and low sediment connectivity index. The Sarbaz and Nahang upper catchments showed strong differences in sediment connectivity (Fig. 9a). Even though the Sarbaz and Nahang river basins have almost identical relief and slope (Fig. 5b, c), however, exposure of olistostrome cover changes sediment connectivity (Fig. 9a) and drainage patterns from Sarbaz to Nahang Catchment (Fig. 1b). In fact, olistostrome as an erodible chaotic lithology is widely distributed and influenced the sediment connectivity in the upper catchment of Sarbaz, but decreases toward the east and Nahang catchments.

The sediment connectivity is in agreement with Melton's ruggedness (Figs. 4d, and 8), while this is in contrast with drainage density (Figs. 4d and 9a). This index shows mostly a high value in the Inner, and western part of Coastal-rough, and intermediate and low values in the Outer and Coastal-plain Makran zones, respectively. These are consistent with the structural pattern, thus reflect more erosional, erosional-depositional (hybrid), and depositional patterns, respectively (Figs. 1a and 9a). It is worth mentioning that the western Coastal-rough Makran reaches its maximum development toward the north (Fig. 1a), where the topographic metrics are higher than the eastern Makran as evidenced by the sediment connectivity (Figs. 5 and 9a).

Discussion

Climate impact on the drainage pattern

An increase in rainfall intensity especially in dry areas can be associated with the rapid development of drainage density, erosion, and sediment supply (Tucker and Slingerland 1997). However, this is not consistently observed from the Inner to Coastal Makran and from the west to the east of Iranian Makran, where drainage density and mean annual precipitation have weak inverse correlations (Fig. 4a, d). Large floods (Fig. 3b) are exceptions, causing the Makran low topography Coastal-plain to respond more than other parts of Makran in a short time, but in general, precipitation is not the main controlling factor of the drainage density in Makran (Figs. 1b and 4a, d). Despite the mostly dendritic pattern of rivers in the Coastal-plain, the catchment parameters and pattern of rivers are constantly changing by flood or drought, as they are primarily ephemeral rivers.

According to several studies of deep and shallow marine sediments from the Gulf of Oman, Arabian Sea, and cave sediments in northern Oman, climate variation has been observed since the Early Holocene with periods of humid (Early Holocene, Fleitmann et al. 2007), dry (Late Holocene, Cullen et al. 2000; He et al. 2020), and arid/semi-arid (present-day, Kehl 2009; Bourget et al. 2010) conditions. Unlike the Present-day climate with minimal impact, the

Early Holocene humid climate might be one of the important controlling factors in drainage pattern development, where it caused erosion and incision to increase. However, the influence of climate on vegetation and thus erosion rate is not well understood. Additionally, the Makran coast was influenced by relatively low-stand sea level during the last glacial period and high sea level during the Holocene, which may have impacted river patterns, especially along the Coastal-plain (Bourget et al. 2010). However, in the present day, the Coastal-plain lacks features like deep incising valleys. Most likely, simultaneous interaction between coastal uplift rate and sea level fluctuations control the Makran rivers base-level.

Lithological impact on the drainage pattern

Drainage patterns can be controlled by lithology of the catchment, where the various rock types respond to erosion differently (e.g. Keller 1986; Vijith et al. 2017). Among the sedimentary cover (succession of deep marine turbiditic sandstone and shale to shallow marine marls and deltaic sandstones) of the Iranian Makran (Figs. 1a and 2), shales and marls are very sensitive to erosion, making them one of the most important sources of sedimentary budget in catchments (e.g. Bouma and Imeson 2000). Therefore, the Coastal-plain Makran with dominant marly bedrocks (Fig. 7e, f) has shown more development of drainage networks, where the density of rivers is more remarkable than other tectono-stratigraphic zones of Iranian Makran (Fig. 4d). Although there is no rising or falling trend of drainage density from west to east Coastal-plain, they are consistent with marl outcrops distribution (Figs. 1a, 2 and 4d). The erosional pattern of marls in a dry climate condition (heavy rainfall in a short period) of Makran, caused to development of a badland topography (hundreds of square kilometres; Normand et al. 2019a) and dendritic river pattern in the Coastal-plain (Fig. 1a). However, the presence of conglomerate, sandstone, or consolidated Quaternary deposits as a cap-rock in the western part of Coastal Makran, prevents rapid erosion and therefore the development of badland morphology (Normand et al. 2019a). Dendritic drainage pattern displays no structural control, can be eroded easily in all directions, and occur where the lithology is homogeneous (Zernitz 1932; Feldman et al. 1997; Twidale 2004). Similarly, the dendritic pattern developed largely on Inner, Outer, and Coastal-rough Makran, where their lithological and structural patterns were partly covered by the olistostrome (thick massive weak-consolidated sediment with very bad sorting, and without any internal structures and bedding; Figs. 1 and 7e). This massive chaotic cover (olistostrome) is lacking in the Pakistani Makran, where the trellis pattern is dominant (Burg 2018).

Furthermore, lithology along with relief and slope influence the depth of incision (e.g. Keller 1986), thereby enhancing deep vertical incision through the sandstone bedrock in the Inner and Outer Makran zones (for example the Jegin River with deeply incised channel; Figs. 2 and 8b), and lateral river migration (meandering) particularly in the Coastal-plain with dominant marl lithology.

Taken together, lithology has a significant impact on drainage patterns in combination with topography and tectonic.

Topographic impact on the drainage pattern

The weak inverse correlations between drainage parameters (area, length, and drainage density) and topographic metrics (mean relief and slope) across the Inner and Coastal-rough Makran (Figs. 6a, c and 9a) imply favourable areas for erosion (Howard 1997; Dragičević et al. 2018). This relationship is mostly attributed to different channelization stages that reflect the extension and integration of existing channels (Lin and Oguchi 2004). By contrast, the Outer Makran with weak positive correlations for those parameters suggests a slower eroding area than the Inner and Coastal-rough Makran. These interpretations may bring biases since topography contributes significantly to the pattern of drainage and erosion (e.g. Burbank and Anderson 2011). Generally, the topographic metrics are decreasing from Inner to Outer Makran (except Jegin and Gabrik Catchments with thick deltaic sandstones and high topography), however, the main thrust fault (Chah Khan Thrust; Figs. 1a and 2) along the strike of Coastal-rough Makran (mainly Fanuj, and Nikshahr Catchments; Fig. 1) create a sudden increase in topography. Therefore, the Outer Makran exhibits a depression, where the sediment supplies from Inner Makran are trapped in the intra-mountain basins. Accordingly, the erosional pattern is more dominant through the Inner Makran (except Nahang catchment, Figs. 7a, b and 9a), while eastern part of Outer Makran (Sarbaz catchment, Fig. 9a), and Coastal Makran display hybrid patterns (more erosional in high topography Coastal-rough and depositional in low topography Coastal-plain; Figs. 5 and 9a). In addition, catchments with high Melton ruggedness values (>0.50) are more prone to instability and debris flow production (Bovis and Jakob 1999; Wilford et al. 2004). This is mainly identified in the strongly deformed Inner Makran (Fig. 7a, b) whit tight folds and denser thrust fault systems (Fig. 1a), as Haghipour and Burg (2014) reported knickpoint related to debris flow in the upper catchment of Fanuj (in the border of North and Inner Makran, concordance with Bashakerd Thrust, Fig. 1a). Contrary to this, Melton's ruggedness value decreases from Coastal Makran with the gentle-fold system to the less deformed flat Coastal-plain (<0.3), which is prone to flooding and indicates more flooding influence. The Melton

ruggedness values between 0.3 and 0.5 are predominantly set with Outer Makran (Fig. 7c), which is an intermediate zone with both mentioned possibilities but to a lesser degree. In general, weak inverse to moderate positive catchment-topographic/climatic correlations across the Iranian Makran reveal that tectonics and topography are key factors in drainage evolution coupled with lithology and precipitation.

Tectonic impact on the drainage systems

Thrust fault-related fold impact

The north dipping Makran thrust fault systems with west–east strike (i.e. Fig. 7g) play an important role in the pattern of drainage networks, particularly those corresponding to the tectonic boundaries of Makran zones (Figs. 1 and 2). The north to south draining rivers are perpendicular to the main thrust faults (Fig. 1), which form fault-related anticlines and act as barriers to the main rivers, thereby increasing drainage density and river length in the uplifted blocks (Figs. 8a and 10a). Therefore, downward blocks (footwalls) act as large-scale synformal basins, accumulating eroded detritus (e.g. the Outer Makran relative to the Inner Makran; Figs. 9 and 10a). In case of the Sarbaz River with two main streams to the west and east in the upper and middle catchment (Inner and Outer Makran; Fig. 1), the footwall of CKT (Fig. 1a) serves as a large synformal basin in the lower catchment (Coastal-plain Makran maximum northward extension; Fig. 1a), bringing two streams together to form the main trunk channel for the Sarbaz River. On the other hand, the drainage pattern variations from the dominant dendritic in the west to the dominant trellis in the east (mainly in Pakistani Makran; Fig. 8a), could be explained by the following reasons due to the thrust faulting:

The west Makran is distinguished by the presence of several long-wavelength synclines (large piggy-back basins) and anticlines with thick sandstone sequences from the east Iranian Makran. The wavelengths of these synclines (Fig. 1a) increase from north to south. They probably formed due to rotation of thrust fault during movement on the frontal thrust. These piggy-back basins are characterized by syn-sedimentary growth strata (Burg and Mohammadi 2015). These synclines have W-E orientation orthogonal to the bulk shortening direction for most of the length of Makran and changed to NW–SE orientation, becoming parallel to the Minab-Zendan fault (Fig. 1a). Therefore, the general structural pattern of Makran with W-E strike of thrust fault-related fold system changes to NW–SE strike in the west

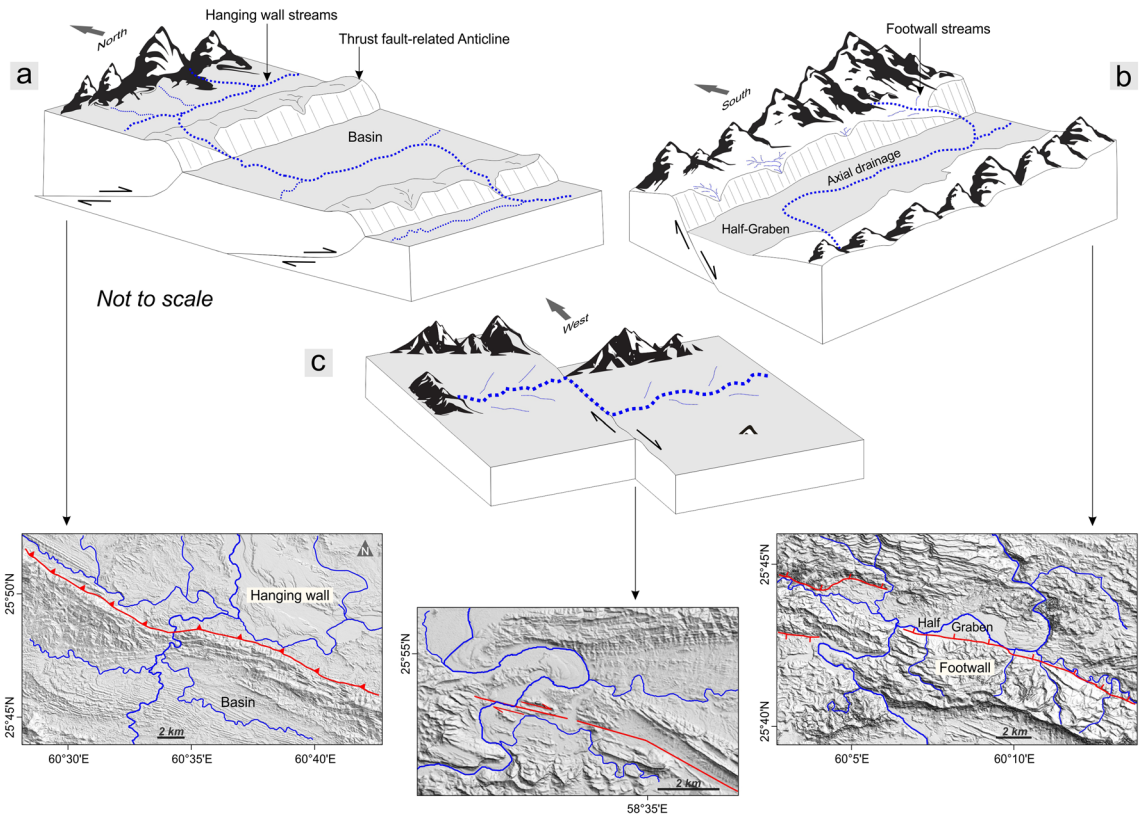

Fig. 10 **a** Schematic block-diagrams (upper part) and TanDEM-X 12.5 m images (lower part) of **a** thrust, **b** normal, and **c** dextral strike-slip faulting across the Iranian Makran. The location of TanDEM-X images is presented in Fig. 2 (white rectangles)

Iranian Makran, which caused to complete pinch-out of the Inner Makran zone in the west of Iranian Makran. This dominantly influenced the drainage pattern of west Makran, a region prone to the dendritic pattern with dominant erosional features (Fig. 1b). In addition, the majority of western Makran small rivers near to the Jegin River Catchment are characterized by high k_{sn} (Fig. 8a), where the topography is higher than the eastern part (Fig. 5). This region is located on the hanging wall of Minab-Zendan Fault zone, which is structurally an oblique dextral-reverse fault and is the surface expression of a deep flower-structure (Regard et al. 2004, 2005).

East–west ward elongate valleys (parallel to main thrust faults) specifically in the eastern part of Iranian Makran (mainly Nahang Catchment) creating a trellis pattern, which is a common characteristic of fold and thrust belt mountains (e.g. Howard 1967; Twidale 2004) such as Zagros (Rangzan and Iqbaluddin 1995), Appalachian Mountains (Kochel 1990; Aravinda and Balakrishna 2013) and Pakistani Makran (Burg 2018). Headward erosion is significant in trellis pattern evolution and is widely invoked in explanations of river capture (Bishop 1995; Twidale 2004). Accordingly, the Pakistani Makran may have captured the Nahang River (Fig. 1b).

The geomorphological indices used in this work suggested that the thrust fault systems are slightly active or no active since the river valleys are in old stages of incision and tend to lateral extension (Fig. 8b). This evidence can reflect tectonically steady structural development in the Inner and Outer Makran as noted by Haghipour et al. (2012) and Burg (2018). However, an exception of V-shaped valleys with W/D < 10 was observed in the Nikshahr River on the hanging wall of Lashar Thrust (Fig. 8b). This may not related to the activity of Lashar Thrust due to lack of seismicity (Fig. 8a inset), however, the absence of seismicity does not mean that the structure is not active, it may have a very high recurrence period, or the structure may be growing at a very low rate. The presence of erosive olistostrome in the footwall of Lashar Thrust (Fig. 1a) most probably increased the incision depth in the hanging wall of Lashar Thrust (Fig. 8b).

Normal fault impact

Coastal Makran is the location of normal faulting (Figs. 1a and 2) since the slab rollback of subducting plate started in the Late Miocene-Pliocene (e.g. Burg et al. 2013) and caused N-S extension of the Makran (e.g. Masson et al. 2007). As a result of the Late Quaternary normal faulting (Fig. 7h, i) and related half-grabens (Fig. 10b), local changes of elevation and relief occurred along the main trunk of some rivers in the Coastal-rough Makran (Nikshahr, and Konarak river basins, Fig. 10b). Therefore, the aforementioned rivers started active deep incisions, and exhibit V-shaped valleys with locally high k_{sn} (Fig. 8a). This is consistent with the significant decrease in the W/D ratio (< 10) compared to the Inner and Outer Makran zones with W/D > 10 (Fig. 8b). The drainage system in the vicinity of the normal faults displays dendritic pattern and asymmetric distribution with respect to the main axial valley (Figs. 8a and 10b). The drainage density is relatively higher in the footwalls (Fig. 10b) compared to the downward blocks, which form half-graben (Fig. 10b). Since the normal faults are active in the Makran region (Normand et al. 2019a, b), the half-grabens act as the intra-mountain basins, and trap a coarser detritus of eroded sediments (Leeder and Jackson 1993) similar to the lower catchment of Nikshahr River (Figs. 9 and 10b). In addition, half-graben influenced drainage patterns locally and caused axial-drainage parallel to the normal fault strikes (Fig. 10b). Similar pattern reported from the extensional setting with normal faults such as the western United States (e.g. Nevada; Peakall 1998) and central Greece (Goldsworthy and Jackson 2000). Overall, the normal faults are the active structure across the Iranian Coastal Makran (Fig. 8a inset). The presence of normal faults in the Coastal-plain Makran, where they cut and deformed the Pleistocene uplifted coastal terraces, is the geological evidence for the activity of Makran normal faults (Fig. 7j; Normand et al. 2019a).

Additionally, the unknown dip-slip faults in the middle and lower catchments of Jegin and Gabrik (Fig. 8a) that were previously mapped as thrust faults in the Taherui 1:250,000 geological map (Geological Survey of Iran) are most likely normal faults (Figs. 1a, 2 and 8a). According to the northward direction of Makran subduction, all thrusts are expected to represent a northward-dip, while they are mapped as southward dipping thrusts. On the other hand, thrust faults in the Outer Makran zone show no deeply incised valleys (except N1 and N2 due to the olistostrome; Fig. 8b), while the aforementioned faults seem to behave as active normal faults with a deeply incised valleys along the Coastal-rough Makran.

Strike-slip fault impact

The majority of Makran strike-slip faults are minor scale and have minimal impact on topography across the Inner and Outer Makran, including conjugate strike-slip faults as well (Figs. 2 and 7n). On the contrary, the Coastal Makran is highly influenced by these structures (Figs. 7l, m and 10c), but their role is hard to assess because of low topography and alluvial sediment cover. These faults are strike-slip and have cut the Neogene sediments in the Coastal-plain (Figs. 1a and 7m). However, the strike, offset and role of the aforementioned strike-slip fault(s) remain indistinct across the Coastal-plain Makran. On the other hand, the Minab earthquake (Irar, 11 May 2013, Fig. 8a inset) with Mw 6.1 provides evidence for the surface

deformation (Fig. 7k), caused by a strike-slip fault roughly perpendicular to the Minab-Zendan Fault zone (Penney et al. 2015).

Pattern of sediment connectivity index and water-erosion hazard

In general, the sediment connectivity pattern has changed toward the east Makran in accordance with the development of thrust fault-related fold systems, exhibiting a correlation with the development of higher connectivity parallel to the mentioned geological structures in the W-E strike (Fig. 9a, b). Combining the aforementioned factors with the sediment connectivity index, suggest that Sarbaz Catchment has the highest potential of sediment supply among all the catchments, since it is a perennial river with a large catchment area and density, overlain by erosive marls (Figs. 2, 4 and 9a). The Jegin and Gabrik Catchments have a high potential of sediment supply and mass-flow, but they are seasonal rivers and mostly covered by sandstone, thus compared to the Sarbaz catchment are in the second order. This potential decreases from Sedij to Fanuj and Nikshahr Catchments. Nahang Catchment and Coastal-plain Makran are more depositional due to syncline structure and low topography (Fig. 9a, b), respectively (Fig. 1a, b). Arid climate and low vegetation cover of Makran make all rivers prone to flooding and mass-flow production during intense rainfall of December to March, as well as very rare rainfall during summer caused by tropical storms. The low topography Coastal-plain is a favorable place to drown by flood and mass flow. Tidal oscillations and waves also contribute to sediment production through uplifted coastal terraces erosion, which could be considered as part of the planning for the urban and industrial development of the Makran coastal zone, particularly in the eastern Iranian Makran with large infrastructures and human population. On the other hand, considering the long-term mean annual rainfall (Fig. 3c), we suggest that the Fanuj and Sarbaz upper Catchment, Jegin and Gabrik Catchments are more prone to mudflows or debris flow on a large scale.

Together, the Inner and Outer Makran typically have dominant north-dipping thrust faults that exhibit high sediment connectivity in their hanging wall, where relief has increased relatively compared to the footwall (Fig. 9b), with the exception of Costal-rough Makran. Relief and topography in the Coastal-rough Makran are mostly controlled by mini-basins and folded massive deltaic sandstones in large-scale (Fig. 2). However, there is no special sediment connectivity pattern in the hanging wall and footwall of the Coastal Makran with normal faults (north and south dipping), where the local and disconnected normal faults are scattered with north and south-dips (Fig. 9a).

Implication for drainage evolution in active accretionary wedges

Drainage pattern and landscape evolution in active accretionary wedges are dominantly depends on the geometry of wedges (e.g. Davis et al. 1983; Viaplana-Muzas et al. 2015). Rivers in accretionary wedges flow from the older, high elevated accreted zone to the younger lower relief zone by crosscutting thrust faults, notably forming trellis river patterns (e.g. Pakistani onshore Makran) similar to fold and thrust belts (e.g. Zagros Mountain; Rangzan and Iqbaluddin 1995). However, in some accretionary wedges, olistostromes overlying the geological structures, forming synformal depocenters (minibasins; Burg et al. 2008; Ruh et al. 2018), changing rock strenght, and thus the river morphology becomes more dendritic such as in the Iranian onshore Makran (Fig. 1b) and Central Andes in Peru (De Jong 1974; Karátson et al. 2012). In the mature accretionary wedges due to slab rollback, extensional tectonic regimes and normal faulting are induced, which can increase river channel depth and incision in the younger parts of active accretionary wedges (e.g. Hellenic trench in the eastern Mediterranean; onshore Makran; Ring et al. 2010; Normand et al. 2019a). On the other hand, the uplifted coast of accretionary wedges (e.g. Central Andes in Chile and Peru; onshore Makran; e.g.Marquardt et al. 2004; Saillard et al. 2011; Normand et al. 2019a) also affects drainage patterns and coastal plain development by changing the base-level of rivers and consequently river incision. Taken together, these geological structures are the major drivers of fluvial landscape evolution in accretionary wedges.

Our findings reveal a considerable impact of regional tectonic and geological structures in combination with topography and lithology on drainage network evolution and sediment yield across the onshore Iranian Makran as a world-scale active accretionary wedge. In addition, the evolution of fluvial landscapes within the accretionary wedges is not homogeneous because geological structures are impacted differently across distinct domains of wedges over time.

Conclusion

The present study evaluated the main drivers of drainage pattern development in onshore Iranian Makran. The following conclusions have been made:

- Transitional changes in Makran rivers trend and pattern from dominant N-S flowing rivers with dendritic pattern in the west (Iranian Makran) to dominant E-W flowing rivers with trellis pattern in the east (Pakistani Makran) correspond to the change of the tectono-mor-

phologic style of Makran from west to east. In fact, the Sarbaz River Catchment in the eastern Iranian Makran serves as a transitional zone between west Makran with several mini-basins and a large olistostrome cover, and east Makran with well-developed thrust fault-related fold system.

- Geological structures including thrust fault-related folds, normal fault-related half grabens, mini-basins and growth strata, and olistostrome cover are the main driver of drainage pattern development in the Iranian onshore Makran. As a secondary factor, the impact of lithology (more erosive marls) and large river floods are considerable in drainage patterns developments.
- The catchment-topographic metrics show river systems are not in equilibrium in the westernmost and easternmost of Iranian Makran, while the central part of the region appears to be in a semi-equilibrium condition.
- The river channel steepness (k_{sn}) pattern and W/D ratio highlight the activity of normal faults in the Coastal Makran, where the rivers are in the young phase of incision.
- The sediment connectivity index shows that the dominant erosional pattern in the western Iranian Makran transitionally changes to more depositional pattern in the eastern Iranian Makran with several scattered normal fault-related intra-mountain depositional basins. Although sediment connectivity index has decreased toward the east Iranian onshore Makran, there is a correlation between higher connectivity and the development of thrust fault-related fold systems on the W-E strike.

Supplementary Information The online version contains supplementary material available at https://doi.org/10.1007/s00531-022-02270-6.

Acknowledgements This work was supported by Istanbul Technical University (İTÜ)/BAP project MAB-2020-42407, and Iran's National Elites Foundation (no. 101/71460, no. 101/71624). Thanks to German Aerospace Centre (DLR, Germany) for providing TanDEM-X datasets under proposal DEM_GEOL3191. The authors thank Lucía Sagripanti and an anonymous referee, as well as Topic Editor Laura Giambiagi for their insightful and constructive comments, which improved the initial manuscript. Thanks also go to Prof. Ulrich Riller for his efficient and thoughtful work as Editor-in-Chief.

Data Availability The TanDEM-X 12.5 m images used in this study are available through the German Aerospace Center (https://tandemx-science.dlr.de/). All modern climate data appears in the main body of the text, and supplementary material comes from the Meteorological stations, Water Resources Management Company of Iran (TAMAB).

Declarations

Conflict of interest The authors declare that they have no known competing financial interests or personal relationships that could have appeared to influence the work reported in this paper.

References

Alavi M (2007) Structures of the Zagros fold-thrust belt in Iran. Am J Sci 307:1064–1095

Ambraseys N, Melville C (1982) A history of persian earthquakes cambridge univ. Press, New York

Aravinda P, Balakrishna H (2013) Morphometric analysis of Vrishabhavathi watershed using remote sensing and GIS. Int J Res Eng Technol 2:514–522

Back S, Morley CK (2016) Growth faults above shale–Seismic-scale outcrop analogues from the Makran foreland, SW Pakistan. Mar Pet Geol 70:144–162

Beechie TJ, Pollock MM, Baker S (2008) Channel incision, evolution and potential recovery in the Walla Walla and Tucannon River basins, northwestern USA. Earth Surf Proc Land 33(5):784–800

Bishop CM (1995) Neural networks for pattern recognition. Oxford university press. p. 477

Borselli L, Cassi P, Torri D (2008) Prolegomena to sediment and flow connectivity in the landscape: a GIS and field numerical assessment. CATENA 75:268–277

Bouma N, Imeson A (2000) Investigation of relationships between measured field indicators and erosion processes on badland surfaces at Petrer, Spain. CATENA 40:147–171

Bourget J, Zaragosi S, Ellouz-Zimmermann S, Ducassou E, Prins M, Garlan T, Lanfumey V, Schneider J-L, Rouillard P, Giraudeau J (2010) Highstand vs. lowstand turbidite system growth in the Makran active margin: Imprints of high-frequency external controls on sediment delivery mechanisms to deep water systems. Mar Geol 274:187–208

Bovis MJ, Jakob M (1999) The role of debris supply conditions in predicting debris flow activity. Earth Surf Proc Land 24:1039–1054

Bracken LJ, Turnbull L, Wainwright J, Bogaart P (2015) Sediment connectivity: a framework for understanding sediment transfer at multiple scales. Earth Surf Proc Land 40:177–188

Bull WB (2011) Tectonically active landscapes. John Wiley & Sons, p. 320

Burbank DW, Anderson RS (2011) Tectonic geomorphology. John Wiley & Sons, p. 460

Burg J-P (2018) Geology of the onshore Makran accretionary wedge: synthesis and tectonic interpretation. Earth Sci Rev 185:1210–1231

Burg J-P, Mohammadi A (2015) ETH reconnaissance excursion in Western Makran, November 2015. Internal report of ETH Zurich. p. 47

Burg JP, Bernoulli D, Smit J, Dolati A, Bahroudi A (2008) A giant catastrophic mud-and-debris flow in the Miocene Makran. Terra Nova 20:188–193

Burg J-P, Dolati A, Bernoulli D, Smit J (2013) Structural style of the Makran Tertiary accretionary complex in SE-Iran, Lithosphere dynamics and sedimentary basins: The Arabian Plate and analogues. Springer, pp. 239–259

Byrne DE, Sykes LR, Davis DM (1992) Great thrust earthquakes and aseismic slip along the plate boundary of the Makran subduction zone. J Geophys Res Solid Earth 97:449–478

Cavalli M, Trevisani S, Comiti F, Marchi L (2013) Geomorphometric assessment of spatial sediment connectivity in small Alpine catchments. Geomorphology 188:31–41

Crema S, Cavalli M (2018) SedInConnect: a stand-alone, free and open source tool for the assessment of sediment connectivity. Comput Geosci 111:39–45

Cullen HM, Demenocal PB, Hemming S, Hemming G, Brown FH, Guilderson T, Sirocko F (2000) Climate change and the collapse of the Akkadian empire: evidence from the deep sea. Geology 28(4):379–382

Cyr AJ, Granger DE, Olivetti V, Molin P (2010) Quantifying rock uplift rates using channel steepness and cosmogenic nuclide–determined erosion rates: examples from northern and southern Italy. Lithosphere 2(3):188–198

Dales M, Reed D (1989) Regional flood and storm hazard assessment. Wallingford, Institute of Hydrology, (IH Report No.102), p. 159

Davis D, Suppe J, Dahlen FA (1983) Mechanics of fold-and-thrust belts and accretionary wedges. J Geophys Res Solid Earth 88(B2):1153–1172

De Jong KA (1974) Melange (Olistostrome) near Lago Titicaca. Peru AAPG Bulletin 58(4):729–741

DiBiase RA, Whipple KX, Heimsath AM, Ouimet WB (2010) Landscape form and millennial erosion rates in the San Gabriel Mountains, CA. Earth Planet Sci Lett 289:134–144

Dolati A (2010) Stratigraphy, structural geology and low-temperature thermochronology across the Makran accretionary wedge in Iran. Dissertation, Zürich, Switzerland, Eidgenössische Technische Hochschule (ETH) Zürich, no. 19151, p. 306

Dolati A, Burg J-P (2013) Preliminary fault analysis and paleostress evolution in the Makran Fold-and-Thrust Belt in Iran, Lithosphere dynamics and sedimentary basins: The Arabian Plate and analogues. Springer, pp. 261–277

Dragičević N, Karleuša B, Ožanić N (2018) Improvement of drainage density parameter estimation within erosion potential method. Multidisciplin Digital Publish Institute Proc 2(11):620

Ellouz-Zimmermann N, Lallemant S, Castilla R, Mouchot N, Leturmy P, Battani A, Buret C, Cherel L, Desaubliaux G, Deville E (2007) Offshore frontal part of the Makran Accretionary prism: The Chamak survey (Pakistan), Thrust belts and foreland basins. Springer, pp. 351–366

Farhoudi G, Karig DE (1977) Makran of Iran and Pakistan as an active arc system. Geology 5(11):664–668

Feldman S, Harris SA, Fairbridge RW (1997) Drainage patterns, Geomorphology. Springer Berlin Heidelberg, Berlin, Heidelberg, pp. 284–291

Fleitmann D, Burns SJ, Mangini A, Mudelsee M, Kramers J, Villa I, Neff U, Al-Subbary AA, Buettner A, Hippler D (2007) Holocene ITCZ and Indian monsoon dynamics recorded in stalagmites from Oman and Yemen (Socotra). Quatern Sci Rev 26:170–188

Flint JJ (1974) Stream gradient as a function of order, magnitude, and discharge. Water Resour Res 10(5):969–973

Fritz HM, Blount CD, Albusaidi FB, Al-Harthy AHM (2010) Cyclone Gonu storm surge in Oman. Estuar Coast Shelf Sci 86(1):102–106

Gailleton B, Mudd SM, Clubb FJ, Grieve SW, Hurst MD (2021) Impact of changing concavity indices on channel steepness and divide migration metrics. J Geophys Res Earth Surface 126(10):2020JF006060

Gallen SF, Wegmann KW (2017) River profile response to normal fault growth and linkage: An example from the Hellenic forearc of south-central Crete, Greece. Earth Surf Dyn 5:161–186

Goldsworthy M, Jackson J (2000) Active normal fault evolution in Greece revealed by geomorphology and drainage patterns. J Geol Soc 157(5):967–981

Grando G, McClay K (2007) Morphotectonics domains and structural styles in the Makran accretionary prism, offshore Iran. Sed Geol 196:157–179

Haghipour N, Burg J-P (2014) Geomorphological analysis of the drainage system on the growing Makran accretionary wedge. Geomorphology 209:111–132

Haghipour N, Burg J-P, Kober F, Zeilinger G, Ivy-Ochs S, Kubik PW, Faridi M (2012) Rate of crustal shortening and non-Coulomb behaviour of an active accretionary wedge: the folded fluvial terraces in Makran (SE, Iran). Earth Planet Sci Lett 355:187–198

Haghipour N, Burg J-P, Ivy-Ochs S, Hajdas I, Kubik P, Christl M (2015) Correlation of fluvial terraces and temporal steady-state incision on the onshore Makran accretionary wedge in southeastern Iran: Insight from channel profiles and 10Be exposure dating of strath terraces. Bulletin 127:560–583

Harel MA, Mudd SM, Attal M (2016) Global analysis of the stream power law parameters based on worldwide ^{10}Be denudation rates. Geomorphology 268:184–196

He W, Liu J, Huang Y, Cao L (2020) Sea level change controlled the sedimentary processes at the Makran continental margin over the past 13,000 yr. J Geophys Re Oceans 125:e2019JC015703

Heidarzadeh M, Pirooz MD, Zaker NH, Yalciner AC, Mokhtari M, Esmaeily A (2008) Historical tsunami in the Makran Subduction Zone off the southern coasts of Iran and Pakistan and results of numerical modeling. Ocean Eng 35:774–786

Hoffmann G, Rupprechter M, Al Balushi N, Grützner C, Reicherter K (2013) The impact of the 1945 Makran tsunami along the coastlines of the Arabian Sea (Northern Indian Ocean)–a review. Z Geomorphol 57:257–277

Horton RE (1932) Drainage-basin characteristics. EOS Trans Am Geophys Union 13:350–361

Horton RE (1945) Erosional development of streams and their drainage basins; hydrophysical approach to quantitative morphology. Geol Soc Am Bull 56:275–370

Howard AD (1967) Drainage analysis in geologic interpretation: a summation. AAPG Bull 51:2246–2259

Howard AD (1997) Badland morphology and evolution: Interpretation using a simulation model. Earth Surface Proc Landforms 22:211–227

Hunziker D, Burg JP, Bouilhol P, von Quadt A (2015) Jurassic rifting at the Eurasian Tethys margin: Geochemical and geochronological constraints from granitoids of North Makran, southeastern Iran. Tectonics 34:571–593

Jackson J, Leeder M (1994) Drainage systems and the development of normal faults: an example from Pleasant Valley. Nevada J Struct Geol 16(8):1041–1059

Karátson D, Telbisz T, Wörner G (2012) Erosion rates and erosion patterns of Neogene to Quaternary stratovolcanoes in the Western Cordillera of the Central Andes: an SRTM DEM based analysis. Geomorphology 139:122–135

Kaveh Firouz A (2018) Active Collision Zones: Morphotectonic Analysis, Cosmogenic Nuclide Evidence and Kinematic Modelling of the Turkish-Iranian Plateau and Caucasus Regions, Doctoral dissertation, ETH Zürich

Kaveh FA, Mohammadi A, Lak R (2020) Makran coastal plain deposits (SE Iran), a potential source of aeolian sediments; insights from sedimentology and geochemistry. 2nd International Conference on Oceanography for West Asia, (16, 17 September 2020 Tehran, Iran), pp. 98–101

Kehl M (2009) Quaternary climate change in Iran—the state of knowledge. Erdkunde 63:1–17

Keller EA (1986) Investigation of active tectonics: use of surficial earth processes. Active Tectonics 1:136–147

Kirby E, Whipple KX (2012) Expression of active tectonics in erosional landscapes. J Struct Geol 44:54–75

Kober F, Zeilinger G, Ivy-Ochs S, Dolati A, Smit J, Kubik P (2013) Climatic and tectonic control on fluvial and alluvial fan sequence formation in the Central Makran Range, SE-Iran. Global Planet Change 111:133–149

Kochel RC (1990) Humid fans of the Appalachian Mountains. Alluvial Fans: A Field Approach. Wiley, New York, 109–129

Kopp C, Fruehn J, Flueh ER, Reichert C, Kukowski N, Bialas J, Klaeschen D (2000) Structure of the Makran subduction zone from wide-angle and reflection seismic data. Tectonophysics 329(1–4):171–191

Kukowski N, Schillhorn T, Huhn K, von Rad U, Husen S, Flueh ER (2001) Morphotectonics and mechanics of the central Makran accretionary wedge off Pakistan. Mar Geol 173(1–4):1–19

Leeder MR, Jackson JA (1993) The interaction between normal faulting and drainage in active extensional basins, with examples from the western United States and central Greece. Basin Res 5(2):79–102

Leggett JK, Platt J (1984) Structural features of the Makran fore-arc on Landsat imagery. Marine Geology and Oceanography of Arabian Sea and Coastal Pakistan. Van Nostrand Reinhold, New York 33:44

Lin Z, Oguchi T (2004) Drainage density, slope angle, and relative basin position in Japanese bare lands from high-resolution DEMs. Geomorphology 63:159–173

Mandal SK, Lupker M, Burg JP, Valla PG, Haghipour N, Christl M (2015) Spatial variability of ^{10}Be-derived erosion rates across the southern Peninsular Indian escarpment: A key to landscape evolution across passive margins. Earth Planet Sci Lett 425:154–167

Marquardt C, Lavenu A, Ortlieb L, Godoy E, Comte D (2004) Coastal neotectonics in Southern Central Andes: uplift and deformation of marine terraces in Northern Chile (27 S). Tectonophysics 394(3–4):193–219

Masson F, Anvari M, Djamour Y, Walpersdorf A, Tavakoli F, Daignieres M, Nankali H, Van Gorp S (2007) Large-scale velocity field and strain tensor in Iran inferred from GPS measurements: new insight for the present-day deformation pattern within NE Iran. Geophys J Int 170:436–440

McCall G (1997) The geotectonic history of the Makran and adjacent areas of southern Iran. J Asian Earth Sci 15:517–531

McCall GJ (2002) A summary of the geology of the Iranian Makran. Geol Soc London, Spec Public 195:147–204

McCall GJH, Kidd RGW (1982) The Makran, Southeastern Iran: the anatomy of a convergent plate margin active from Cretaceous to Present. Geol Soc London Spec Public 10(1):387–397

Melton MA (1958) Correlation structure of morphometric properties of drainage systems and their controlling agents. J Geol 66:442–460

Melton MA (1965) The geomorphic and paleoclimatic significance of alluvial deposits in southern Arizona. J Geol 73:1–38

Miller CS, Leroy SA, Collins PE, Lahijani HA (2016) Late Holocene vegetation and ocean variability in the Gulf of Oman. Quatern Sci Rev 143:120–132

Minshull T, White R (1989) Sediment compaction and fluid migration in the Makran accretionary prism. J Geophys Res Solid Earth 94(B6):7387–7402

Mohammadi A (2010) Sedimentology and sedimentary geochemistry of Jazmurian playa. J Arid Biome 1(1):68–79

Mohammadi A, Burg J-P, Guillong M, von Quadt A (2017) Arc magmatism witnessed by detrital zircon U-Pb geochronology, Hf isotopes and provenance analysis of Late Cretaceous-Miocene sandstones of onshore western Makran (SE Iran). Am J Sci 317:941–964

Mohammadi A, Burg J-P, Winkler W, Ruh J, von Quadt A (2016a) Detrital zircon and provenance analysis of Late Cretaceous–Miocene onshore Iranian Makran strata: Implications for the tectonic setting. Bulletin 128:1481–1499

Mohammadi A, Burg J-P, Winkler W (2016b) Detrital zircon and provenance analysis of Eocene–Oligocene strata in the South Sistan suture zone, southeast Iran: Implications for the tectonic setting: Lithosphere 8(6):615–632

Montgomery DR, Brandon MT (2002) Topographic controls on erosion rates in tectonically active mountain ranges. Earth Planet Sci Lett 201:481–489

Montgomery DR, Dietrich WE (1989) Source areas, drainage density, and channel initiation. Water Resour Res 25:1907–1918

Moore ID, Grayson R, Ladson A (1991) Digital terrain modelling: a review of hydrological, geomorphological, and biological applications. Hydrol Process 5:3–30

Morisawa ME (1962) Quantitative geomorphology of some watersheds in the Appalachian Plateau. Geol Soc Am Bull 73(9):1025–1046

Musson R (2009) Subduction in the Western Makran: the historian's contribution. J Geol Soc 166:387–391

Normand R, Simpson G, Herman F, Biswas RH, Bahroudi A, Schneider B (2019a) Dating and morpho-stratigraphy of uplifted marine terraces in the Makran subduction zone (Iran). Earth Surf Dyn 7:321–344

Normand R, Simpson G, Bahroudi A (2019b) Extension at the coast of the Makran subduction zone (Iran). Terra Nova 31(6):503–510

Peakall J (1998) Axial river evolution in response to half-graben faulting; Carson River, Nevada, USA. J Sediment Res 68(5):788–799

Penney C, Copley A, Oveisi B (2015) Subduction tractions and vertical axis rotations in the Zagros-Makran transition zone, SE Iran: the 2013 May 11 M w 6.1 Minab earthquake. Geophys J Int 202:1122–1136

Penney C, Tavakoli F, Saadat A, Nankali HR, Sedighi M, Khorrami F, Sobouti F, Rafi Z, Copley A, Jackson J (2017) Megathrust and accretionary wedge properties and behaviour in the Makran subduction zone. Geophys J Int 209:1800–1830

Peri VG, Haghipour N, Christl M, Terrizzano C, Kaveh-Firouz A, Leiva MF, Pérez P, Yamin M, Barcelona H, Burg JP (2022) Quaternary landscape evolution in the Western Argentine Precordillera constrained by ^{10}Be cosmogenic dating. Geomorphology 396:107984

Rajendran C, Rajendran K, Shah-Hosseini M, Beni AN, Nautiyal CM, Andrews R (2013) The hazard potential of the western segment of the Makran subduction zone, northern Arabian Sea. Nat Hazards 65:219–239

Rangzan KI (1995) Morpho-tectonic study of Zagros structural belt of SW Iran using remote sensing techniques. J Indian Soc Remote Sensing 23:211–224

Regard V, Bellier O, Thomas JC, Abbassi M, Mercier J, Shabanian E, Feghhi K, Soleymani S (2004) Accommodation of Arabia-Eurasia convergence in the Zagros-Makran transfer zone, SE Iran: a transition between collision and subduction through a young deforming system. Tectonics 23:1–24

Regard V, Bellier O, Thomas J-C, Bourles D, Bonnet S, Abbassi M, Braucher R, Mercier J, Shabanian E, Soleymani S (2005) Cumulative right-lateral fault slip rate across the Zagros—Makran transfer zone: role of the Minab—Zendan fault system in accommodating Arabia—Eurasia convergence in southeast Iran. Geophys J Int 162:177–203

Ricou LE (1994) Tethys reconstructed: plates, continental fragments and their Boundaries since 260 Ma from Central America to South-eastern Asia. Geodin Acta 7(4):169–218

Ring U, Glodny J, Thomson WT, S, (2010) The Hellenic subduction system: high-pressure metamorphism, exhumation, normal faulting, and large-scale extension. Annu Rev Earth Planet Sci 38:45–76

Ruh JB, Vergés J, Burg JP (2018) Shale-related minibasins atop a massive olistostrome in an active accretionary wedge setting: Two-dimensional numerical modeling applied to the Iranian Makran. Geology 46(9):791–794

Saillard M, Hall SR, Audin L, Farber DL, Regard V, Hérail G (2011) Andean coastal uplift and active tectonics in southern Peru: 10Be surface exposure dating of differentially uplifted marine terrace sequences (San Juan de Marcona,~ 15.4 S). Geomorphology, 128(3–4):178–190

Scherler D, Bookhagen B, Strecker MR (2014) Tectonic control on 10Be-derived erosion rates in the Garhwal Himalaya, India. J Geophys Res Earth Surf 119(2):83–105

Schlüter HU, Prexl A, Gaedicke C, Roeser H, Reichert C, Meyer H, Von Daniels C (2002) The Makran accretionary wedge: sediment thicknesses and ages and the origin of mud volcanoes. Mar Geol 185(3–4):219–232

Schumm SA (1956) Evolution of drainage systems and slopes in badlands at Perth Amboy, New Jersey. Geol Soc Am Bull 67:597–646
Schwanghart W, Scherler D (2014) TopoToolbox 2–MATLAB-based software for topographic analysis and modeling in Earth surface sciences. Earth Surf Dyn 2:1–7
Schwanghart W, Scherler D (2017) Bumps in river profiles: uncertainty assessment and smoothing using quantile regression techniques. Earth Surf Dyn 5:821–839
Seybold H, Berghuijs WR, Prancevic JP, Kirchner JW (2021) Global dominance of tectonics over climate in shaping river longitudinal profiles. Nat Geosci 14:503–507
Shah-Hosseini M, Ghanavati E, Morhange C, Beni AN, Lahijani HA, Hamzeh MA (2018) The evolution of Chabahar beach ridge system in SE Iran in response to Holocene relative sea level changes. Geomorphology 318:139–147
Smith AG, Fox M, Schwanghart W, Carter A (2022) Comparing methods for calculating channel steepness index. Earth Sci Rev 227:103970
Snead RJ (2002) Uplifted marine terraces along the Makran coast of Pakistan and Iran, Himalaya to the Sea. Routledge, pp. 225–246
Snyder NP, Whipple KX, Tucker GE, Merritts DJ (2000) Landscape response to tectonic forcing: digital elevation model analysis of stream profiles in the Mendocino triple junction region, northern California. Geol Soc Am Bull 112:1250–1263
St-Onge D (2012) Late Wisconsinan morphosedimentary sequences of the lower Coppermine River valley. Nunavut and Northwest Territories Geosci Canada 39(3):132–147
Strahler AN (1964) Quantitative geomorphology of drainage basin and channel networks. Handbook of applied hydrology
Strahler AN (1957) Quantitative analysis of watershed geomorphology. EOS Trans Am Geophys Union 38:913–920
Tucker GE, Slingerland R (1997) Drainage basin responses to climate change. Water Resour Res 33:2031–2047
Tucker GE, Whipple KX (2002) Topographic outcomes predicted by stream erosion models: Sensitivity analysis and intermodel comparison. J Geophys Res Solid Earth 107(B9):ETG-1
Twidale C (2004) River patterns and their meaning. Earth Sci Rev 67:159–218
Valkanou K, Karymbalis E, Papanastassiou D, Soldati M, Chalkias C, Gaki-Papanastassiou K (2020) Morphometric analysis for the assessment of relative tectonic activity in Evia Island. Greece Geosci 10:264
Vernant P, Nilforoushan F, Hatzfeld D, Abbassi M, Vigny C, Masson F, Nankali H, Martinod J, Ashtiani A, Bayer R (2004) Present-day crustal deformation and plate kinematics in the Middle East constrained by GPS measurements in Iran and northern Oman. Geophys J Int 157:381–398
Viaplana-Muzas M, Babault J, Dominguez S, Van Den Driessche J, Legrand X (2015) Drainage network evolution and patterns of sedimentation in an experimental wedge. Tectonophysics 664:109–124
Vijith H, Prasannakumar V, Sharath Mohan M, Ninu Krishnan M, Pratheesh P (2017) River and basin morphometric indexes to detect tectonic activity: a case study of selected river basins in the South Indian Granulite Terrain (SIGT). Phys Geogr 38:360–378
Vita-Finzi C (2002) Neotectonics on the Arabian Sea coasts. Geol Soc London Spec Public 195:87–96
Von Rad U, Berner U, Delisle G, Doose-Rolinski H, Fechner N, Linke P, Lückge A, Roeser HA, Schmaljohann R, Wiedicke M, Block M (2000) Gas and fluid venting at the Makran accretionary wedge off Pakistan. Geo-Mar Lett 20(1):10–19
Wessel B, Huber M, Wohlfart C, Marschalk U, Kosmann D, Roth A (2018) Accuracy assessment of the global TanDEM-X Digital Elevation Model with GPS data. ISPRS J Photogramm Remote Sens 139:171–182
Weyhenmeyer CE, Burns SJ, Waber HN, Macumber PG, Matter A (2002) Isotope study of moisture sources, recharge areas, and groundwater flow paths within the eastern Batinah coastal plain, Sultanate of Oman. Water Res Res 38:21–22
Whipple KX (2004) Bedrock rivers and the geomorphology of active orogens. Annu Rev Earth Planet 32:151–185
Whipple KX, Tucker GE (1999) Dynamics of the stream-power river incision model: implications for height limits of mountain ranges, landscape response timescales, and research needs. J Geophys Res Solid Earth 104(B8):17661–17674
White RS (1982) Deformation of the Makran accretionary sediment prism in the Gulf of Oman (north-west Indian Ocean). Geol Soc London Spec Public 10:357–372
White RS (1983) The Makran accretionary prism. Book chapter
White RS, Louden KE (1982) The Makran continental margin: structure of a thickly sedimented convergent plate boundary: convergent margins: field investigations of margin structure and stratigraphy. AAPG 499–518
Wilford D, Sakals M, Innes J, Sidle R, Bergerud W (2004) Recognition of debris flow, debris flood and flood hazard through watershed morphometrics. Landslides 1:61–66
Willett SD, McCoy SW, Perron JT, Goren L, Chen C-Y (2014) Dynamic reorganization of river basins. Science 343:61–75
Wilson JP (2018) Environmental applications of digital terrain modeling. John Wiley & Sons, p. 360
Wobus C, Whipple KX, Kirby E, Snyder N, Johnson J, Spyropolou K, Crosby B, Sheehan D, Willett S (2006) Tectonics from topography: procedures, promise, and pitfalls. Spec Papers Geol Soc Am 398:55
Zernitz ER (1932) Drainage patterns and their significance. J Geol 40:498–521
Zingaro M, Refice A, Giachetta E, D'Addabbo A, Lovergine F, De Pasquale V, Pepe G, Brandolini P, Cevasco A, Capolongo D (2019) Sediment mobility and connectivity in a catchment: a new mapping approach. Sci Total Environ 672:763–775